Received: 22 February 2024 | Revised: 2 August 2024 | Accepted: 2 September 2024

DOI: 10.1002/ese3.1915

ORIGINAL ARTICLE

Design and performance analysis of portable solar powered cooler for vaccine storage

Vicent Marwa[1,2] | **Thomas Kivevele**[1] | **Baraka Kichonge**[1,3] | **Juma Selemani**[1]

[1]School of Materials, Energy, Water, and Environmental Sciences, The Nelson Mandela African Institutional of Science and Technology, Arusha, Tanzania

[2]Department of Mechanical and Industrial Engineering, Mbeya University of Science and Technology, Mbeya, Tanzania

[3]Department of Mechanical Engineering, Arusha Technical College, Arusha, Tanzania

Correspondence
Thomas Kivevele, School of Materials, Energy, Water, and Environmental Sciences, The Nelson Mandela African Institutional of Science and Technology, P. O. Box 447, Arusha, Tanzania.
Email: thomas.kivevele@nm-aist.ac.tz

Funding information
SOVAS PROJECT; HEET PROJECT

Abstract

The efficacy of vaccine storage is significantly impacted by temperature fluctuations within the cooler, often exacerbated by using phase change materials in existing cooler designs for remote areas. These materials can undergo uneven melting and phase separation, leading to temperature instability and vaccine potency loss. In response to this challenge, the present study introduces a novel design of a portable, locally-made solar-powered cooler optimized for longer storage periods. The cooler's performance in terms of temperature distribution, airflow dynamics, and the coefficient of performance (COP) is meticulously examined through computational fluid dynamics (CFD) simulations. The simulated results were validated using experimental data from the open literature, ensuring accuracy and reliability. The findings indicate that the developed cooler achieves significant improvements over traditional models. For instance, the current model reaches a temperature of +12°C in just 84 min, compared to 208 min, as reported in the literature results. Moreover, the current model reaches a temperature of −12°C in 195 min and it has energy efficient with a COP of 4.5. Statistical analysis further confirms the reliability of the simulation results, with root mean square and mean absolute percentage errors of 6.587 and 24.2%, respectively. Additionally, a comparative study of five insulative materials highlights polyurethane (Po) as the top performer, with a heat transfer performance of 14.3%, followed by feather fiber (Fe) (18.7%), fly ash (Fl) (19.8%), fiberglass (Fi) (21.9%), and coconut fiber (Co) (25.9%). Notably, net present value (NPV) of $689.336 and $448.01 was obtained for economic analysis of the current model over the existing model, showing the feasibility of the study. Hence, the cooler's effectiveness in storing vaccines in isolated regions exceeds that of conventional models, providing a hopeful solution to tackle vital challenges in vaccine distribution and preservation.

KEYWORDS
insulative material, simulation, temperature distribution, vaccine storage

1 | INTRODUCTION

Vaccine demand has increased dramatically in Africa recently.[1,2] Vaccines are temperature sensitive[3] and must be kept in a cold chain between +2°C and +8°C[4,5] to remain potent. However, some vaccines, including COVID-19, go beyond −15°C[6]; as a result, maintaining a cold chain system to deliver vaccines to end users is challenging, increasing the number of unused and mismanaged discarded vaccines.[7] Distribution of the vaccines to the general populace in Sub-Saharan Africa is still tricky, particularly in rural or suburban areas where small towns, pharmacy chains, and hospitals might not have the electricity and necessary facilities to keep the vaccine at the right temperature for a more extended period. Globally, 1.3 billion individuals still lack access to power,[8] the majority of whom live in Africa and Asia,[9] of which 600 Million live in Sub-Saharan Africa.[10] The intermittent and fluctuating electric power supplies, high humidity and extreme ambient temperatures significantly impact vaccine storage.[11] These conditions can compromise the effectiveness and safety of vaccines, as they require consistent and stable storage environments to maintain their potency. Ensuring a reliable power supply and proper climate control is crucial to preserving the integrity of vaccines, preventing spoilage, and safeguarding public health.

Most existing coolers in off-grid systems use phase change materials, for example, ice packs.[12] These materials undergo uneven temperature distribution,[13] supercooling,[14] and cause corrosion,[15] resulting in vaccine potency loss. Therefore, for a continuous supply of cold chains, solar-powered vaccine storage is inevitable in supplementing the absence of electricity. The solar-powered cooler presents an innovative method to address the challenges of remote locations and unreliable power supplies in most remote areas. This innovative approach is particularly valued for its potential to overcome the challenges of using phase change materials. A few studies are available in the open literature on solar-powered vaccine storage cooling processes.[16] designed and fabricated solar vapor compression refrigeration for vaccines and medicine with a 9-L capacity. The results indicated that a minimum storage temperature of 6°C was maintained within the year of operation. Ray et al.[17] conducted a study on the cooling performance of vaccine storage for cylindrical and cuboid boxes integrated with phase change material (SP-50) using computational fluid dynamics (CFD). The results indicated temperature differences within the vaccine cold boxes. The top and corners exhibited higher temperatures compared to the mid surfaces. This was attributed to concentrated heat flux at ambient temperatures of 45°C and 30°C. The differential heat distribution highlighted the importance of considering various factors when designing thermal management systems for vaccine cold boxes. Zhang et al.[18] explored the temperature distribution inside refrigerated containers, created a three-dimensional CFD model, and confirmed that CFD can accurately forecast the temperature distribution inside such containers. This validation enhances the reliability of CFD as a predictive tool in this research. Ng et al.[19] studied temperature-controlled vaccine cold box transportation in cold chains using coolant packs. The results indicated that a larger polystyrene foam box with five coolant packs successfully sustained the desired temperature for up to 23 h. On the contrary, setups involving a polystyrene foam box with four coolant packs and a substantial vaccine cold box with two coolant packs could not maintain temperatures below 8°C for the entire 24-h. However, the major drawback of the configuration was the increased risk of freezing.

Most previous works on solar-powered coolers have focused on large-scale systems,[20] overlooking the development of portable coolers essential for the remote distribution of vaccines. This oversight is particularly critical in regions with poor road infrastructure, especially in the Sub-Saharan area. Reliable, portable, and efficient cooling solutions are paramount to ensure vaccines' practical storage and distribution. The studies on solar-powered systems using CFD research have primarily focused on two areas: forced convection-based containers designed for the storage of vaccines[21] and the analysis of airflow characteristics in various configurations[22] with less emphasize on temperature variation within the cooler and optimization of the insulation materials used. Existing research predominantly focuses on conventional cooling systems,[23] leaving a notable gap in the comprehensive analysis of the thermal performance and efficiency of innovative insulating materials explicitly tailored for solar-powered vaccine coolers. Despite advancements in solar-powered cooling technology, there remains a significant need to understand the effectiveness of various insulating materials in maintaining the ultra-low temperatures required for vaccine storage. Addressing this gap is crucial for enhancing the reliability and efficiency of vaccine storage solutions, particularly in off-grid and resource-limited settings.

In this study, a reliable, portable, and efficient solar-powered cooler was explicitly developed for vaccine distribution in remote areas, and its performance was thoroughly analyzed. The research also evaluated various insulating materials, including feather fiber, fly ash, fiberglass, polyurethane, and coconut fiber, to enhance the cooler's effectiveness. These insulating materials were carefully selected and designed to maintain a distinct

separation between the container's indoor environment and the external ambient conditions. Additionally, the modeling results from this study were used to guide experimental efforts, thereby reducing the number of trials, as well as saving time and costs.

2 | MATERIALS AND METHODS

The components used in this study were categorized into two parts: a power supply unit and a cooling system unit, as shown in Figure 1 and in the numerical model Figure 2. A power supply unit includes a solar panel, solar battery, and charge controller, while a cooling system unit includes a compressor, condenser, evaporator, and capillary tube. This cooling system is embedded with galvanized sheets, aluminum sheets, and polyurethane foam (Po). The outer cover of the cooling system termed a cooler is surrounded by a galvanized sheet material 1.5 mm thick, and an aluminum sheet of 1.5 mm is in the inner cover between the galvanized sheet and aluminum sheet. Polyurethane foam acts as an insulation material of 72 mm. The insulating material significantly impacts an object's ability to resist heat.[24]

Due to the availability of insulation materials in the local market, five categories were found. However, a comparison through simulations was conducted to find the best material to use. The simulation utilized in this work to analyze the heat transfer rate involved five insulation materials, as indicated in Table 1. The best thermal conductivity for cold storage is found in all materials, albeit slight variations exist. Four different external temperatures, 313, 308, 303, and 298 K, were used for CFD steady-state thermal analysis. The simulation used a constant of $2\,W\,m^{-2}\,K^{-1}$ heat transfer coefficient, assuming the ambient temperature was 295 K and the internal temperature was 253 K throughout the simulation. These materials have low thermal conductivity. Additionally, the availability in the local market and low thermal conductivities were the most critical factors during the selection of these insulation materials.

2.1 | Analytical design of vaccine storage

A 30 L of the overall dimensions of the vaccine storage and inside cabinet measurements are $859 \times 565 \times 527$ mm and

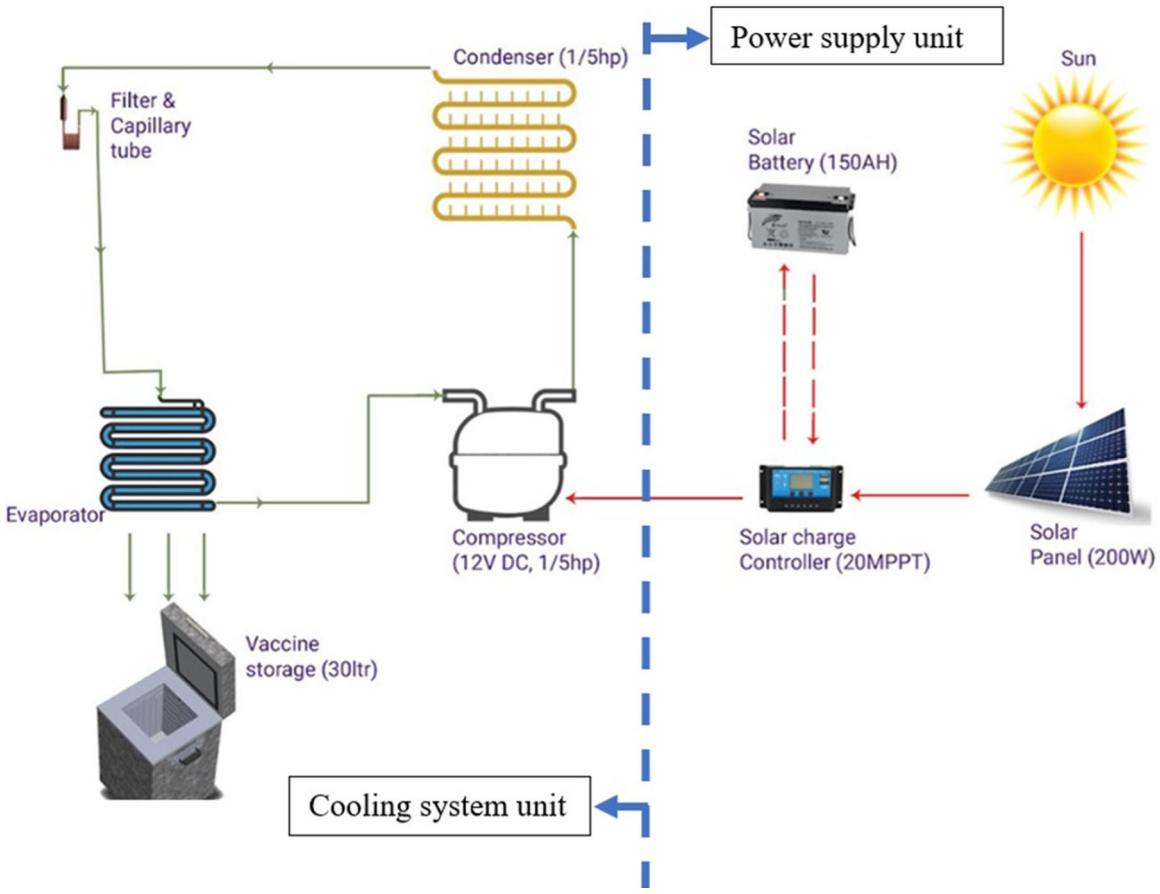

FIGURE 1 A schematic diagram of vaccine storage system key components.

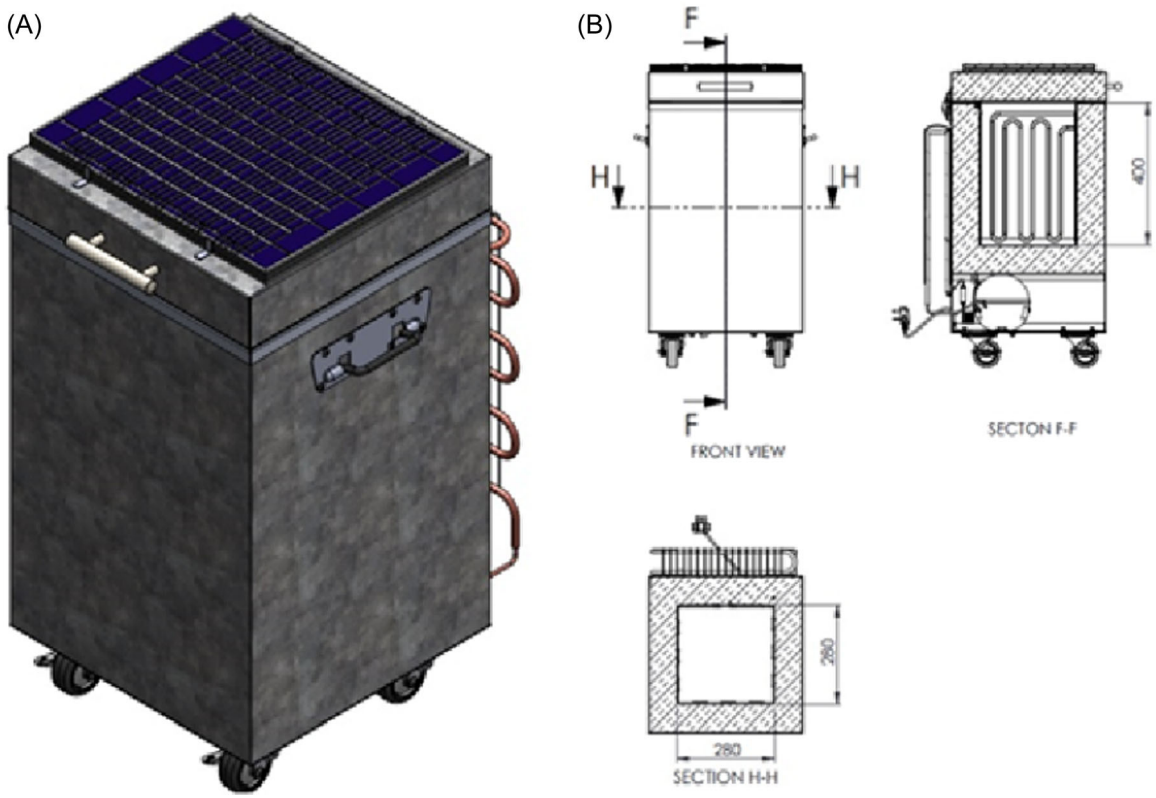

FIGURE 2 Assembly vaccine cooler. (A) Folded placed at the top of the cooler. (B) Cross section view.

TABLE 1 Thermal conductivity of insulation material.

Insulating material	Thermal conductivity ($W\,m^{-1}\,K^{-1}$)	Author
Coconut fiber (Co)	0.048	Kumar[25]
Fiberglass (Fi)	0.04	Pavithra et al.[26]
Fly ash Fiber (Fl)	0.035	Massoudinejad et al.[27]
Feather fiber (Fe)	0.033	Dieckmann et al.[28]
Polyurethane foam (Po)	0.024	Xu et al.[29]

$400 \times 280 \times 280$ mm (height × length × width), respectively. It involves the identification of many significant parts in each design component.

2.1.1 | Determination of the solar panel

A 200 W, 12 V, foldable solar panel has been used. The solar panel's folded dimensions are $435 \times 375 \times 22$ mm (length × width × thickness), making it reasonably portable. Equations (1) and (2) were applied to determine solar panels.[30] To determine the total appliance utilized for the vaccine cooler, sunlight is expected to be present for 6 h every day. The compressor has a power rating of 86 W, so the total appliance utilized will be as follows:

$$\text{power consumption} = \text{daily load} \times \text{peak hour sunshine}, \quad (1)$$

$$\text{number of photovoltaic cell panel needed} = \frac{\text{total photovoltaic cell panel capacity}}{\text{panel size rating}}. \quad (2)$$

According to Atsu et al.,[31] photovoltaic panels can operate effectively for 25 years. However, there are

challenges concerning the durability and performance of these modules that require attention. Factors like panel temperature,[32] system load,[33] dust deposition,[34] irradiance,[35] and sun direction,[36] dust accumulation,[37] shadows,[38] humidity,[39] wind speed,[40] and damaged panels.[41] To prevent these impacts, actions should be implemented such as panel cleaning,[42] solar trackers for sun direction,[43] avoiding even partial shadow,[38] cooling methods for overheating and real-time monitoring for panel damage.[44]

2.1.2 | Storage battery

Two 85Ah deep cycle lead acid batteries keep the cooler for keeping immunizations powered up. The appliance use is assumed to be 16 h per day, days of autonomy (the number of days the system will function without electricity from PV panels) is supposed to be 1, battery loss is assumed to be 0.8, and nominal battery voltage is considered 12. Equation (3) was considered to determine the number of solar batteries used.[45]

$$\text{Battery size} = \frac{\text{total watt} \times \text{hours per day used by appliances} \times \text{days of autonomy}}{0.8 \times \text{nominal battery voltage}}. \quad (3)$$

Sahajwalla and Hossain[46] noted that the battery lifespan typically spans around 15 years, achievable through proper maintenance and care. Factors like discharging batteries to higher depths[47] and exposure to elevated temperatures[48] can impact battery longevity. Maintaining the water level in each battery cell is crucial for its charging and discharging cycles. Keeping the water level at an optimal level requires regular watering; however, both overwatering and underwatering can harm battery life.[42] Periodic discharging and recharging of batteries result in water consumption during charging. Charging should commence only when the battery voltage hits the minimum level.[49] Regular checks on liquid levels in battery cells and adding water to depleted cells as per manufacturer guidelines are necessary. When batteries are part of a PV system, they must be situated in well-ventilated areas without extreme temperatures to ensure optimal performance.

2.1.3 | Charge controller

The charge controller of 12 V, 20 A of maximum power point tracking (MPPT) was selected, of which 25% was considered a safety factor due to the panel producing more power. Equation (4) was used to calculate the size of the charge controller:[50]

$$\text{power} = \text{voltage} \times \text{current}. \quad (4)$$

The charge controller employs MPPT to acquire the ideal solar power necessary for maximizing output.[51] PV panels demonstrate a nonlinear voltage–current profile, with a defined peak power point affected by environmental factors such as temperature and sunlight exposure. Solar panels need to consistently operate at this optimal point to achieve peak power generation, disregarding environmental changes. The MPPT system effectively supervises and adjusts the operational point to boost the power yield from PV panels. The performance of a solar-powered cooler heavily relies on efficient maintenance and durability. Failing to upkeep the system properly can lead to reduced efficiency, increased energy usage, and the risk of system malfunctions in the long run. Consistent maintenance guarantees the optimal operation of the cooler and extends its longevity.

2.1.4 | Compressor

The compressor selected was 12 V, DC hermetic 1/5 hp because this type helps to minimize gas leakage out of the system. Equation (5) was used for the compressor determination.[52]

$$\text{compressor power } (Q_P) = \text{mass flow rate}(\dot{m}) \times \text{work done by compressor } (W_c). \quad (5)$$

A compressor integrates mechanical compression components with an electric motor for efficient operation.[53] Various factors like component quality, operating conditions, and maintenance practices influence the lifespan of a DC compressor. A DC compressor can typically last 10 years under regular operating conditions.[54] Maintaining a DC compressor is crucial for ensuring its longevity and optimal performance. Regular maintenance helps prevent potential issues, such as decreased efficiency, increased energy consumption, and system failures. By conducting routine inspections, cleaning, and servicing, the lifespan of the compressor can be extended to ensure its operation efficiently.

2.1.5 | Condenser

A condenser of dimension length 1160 mm × width 450 mm, 1/5 hp, wire, and tube was selected to enable natural and forced convection to effectively remove heat

from the surface. Equation (6) was used for condenser determination.[55]

$$\text{condenser load } (Q_L) = \text{mass flow rate } (\dot{m}) \times \text{heat by condenser.} \quad (6)$$

2.1.6 | Evaporator

The evaporator has a dimension length of 1200 mm and a width of 40 mm. Aluminum coils were selected because they guard against pinhole leaks, metallic corrosion, and rusty tube sheets. Equation (7) was used to calculate the evaporator sizing.[56]

$$\text{evaporator load } (Q_E) = \text{mass flow rate } (\dot{m}) \times \text{heat by evaporator.} \quad (7)$$

2.1.7 | Coefficient of performance

A cooler's coefficient of performance (COP) is given as 4.5. COP is the ratio of energy taken away from the cold reservoir to the work input. The higher the COP, the more efficient the cooler, the less energy (power) consumption, and therefore reduced running costs. Equation (8) was used to determine the COP of a system.[16]

$$\text{COP} = \frac{\text{refrigerating effect}}{\text{work done by the compressor}}. \quad (8)$$

2.1.8 | Heat transfer across the wall

The heat transfer rate within the wall at the vaccine cooler was determined using conduction and convection calculation formulas. Equation (9) was used to determine the heat transfer rate[57]:

$$Q = \frac{A_w(T_i - T_o)}{\frac{1}{h_i} + \frac{x_A}{k_A} + \frac{x_B}{k_B} + \frac{x_C}{k_C} + \frac{1}{h_o}}. \quad (9)$$

where A_w is the surface area of the wall (m^2), h_i the heat transfer coefficeints at the inner ($W\,m^{-2}\,K^{-1}$), h_o the heat transfer coefficients at the outer ($W\,m^{-2}\,K^{-1}$), x_A the thickness of aluminum sheet (m), x_B the thickness of galvanized sheet (m), x_C the thickness of polyurethane foam (m), k_A the thermal conductivity of aluminum sheet ($W\,m^{-1}\,K^{-1}$), k_B the thermal conductivity of galvanized sheet ($W\,m^{-1}\,K^{-1}$), k_C the thermal conductivity of polyurethane foam ($W\,m^{-1}\,K^{-1}$), T_i the Inner temperature (K), and T_o the outer temperature (K).

2.1.9 | Evaluation methods

The length and information level of the experimental data set for simulation model evaluation must be carefully examined since they have a significant impact on model performance. Thus, techniques for identifying crucial time intervals in observations with the most information for parameter identification may provide valuable recommendations when choosing the evaluation data series.[58] The statistical performance measures were used to compare the simulated model outputs to the numerical data to estimate error using the root mean squared error (RMSE) and mean absolute percentage error (MAPE). The RMSE formula computes the squared error of the prediction when compared to observed values, as well as the squared root of the summation value. It provides high confidence in the model's anticipated values. Equations (10) and (11) were used to evaluate the root mean square error and mean average percentage error.[59]

$$\text{RMSE} = \sqrt{\sum_{i=1}^{n} \frac{(\text{predicted value-observed value})^2}{\text{number of obervation}}} \quad (10)$$

and

$$\text{MAPE} = \frac{1}{n}\sum_{t=1}^{n}\left|\frac{\text{observed value-predicted value}}{\text{observed value}}\right| \quad (11)$$

.

2.2 | CFD simulation of the cooler

CFD is a fluid dynamic that studies heat transfer and fluid flow problems. Numerical methods and algorithms are used to examine and solve problems. The model and analysis of CFD are utilized to analyze fluids in various systems.[60] The fundamental advantage of employing numerical methods is that the problem is resolved by discretizing it based on a set of parameters. A mathematical model represents the actual physical system, which can be solved and examined.[61]

The CFD investigation's foundation is modeling vaccine storage in the ideal cooler. ANSYS version 2021R2 software was utilized to run the simulation, while ANSYS FLUENT was used to mesh and design a modeler to model the cooler. It is significant to note that a model can created and simulated using CFD without the model ever being built. Due to the availability of effective computer systems, numerical modeling techniques, including but not limited to CFD approaches, have become well-known in the academic and industrial sectors. By employing CFD

simulations to understand physiochemical parameters inside the model and optimize system design and operation, the system can be characterized with fewer experiments. Simulations generate spatial and temporal profiles of many system parameters that are either difficult to measure or can only be obtained through pricy experiments.

2.3 | Details of mesh

The geometric model was meshed using ANSYS Meshing version 2021R2. Figure 3 displays the cooling cabinet's mesh and three-dimensional (3D) geometric domains. The names of the six walls of the cooling cabinet are presented in Figure 3a, a geometric illustration. The cooling cabinet's width is along the x-axis, its depth is along the *z*-axis, its height is along the *y*-axis, and gravity operates in the negative *y*-axis. The six walls that comprise the CFD geometry are designated top, bottom, back, side, and front. They consider natural convection from environmental interactions and heat transfer through conduction in the insulating material. The condenser is fixed on the back of the vaccine storage structure.

An unstructured grid of tetrahedron elements was constructed, and the results are displayed in Table 2. The size or distinctive length of each element in the mesh is referred to as 3 mm, resulting in the element number of 6,792,615 of the nodes 9,468,051 employed as the initial meshed values of the geometry domain. The mesh quality was medium, with a growth rate of 1.2.

2.3.1 | Mesh generation

The mesh quality significantly impacts the accuracy of the solutions in CFD simulations.[62] Geometry must include grids or meshes, and meshing is a crucial step in the CFD process. The method selected at the meshing stage determines the mesh's quality. Mesh divides a 3D fluid system model into thousands of smaller flow domains, each of which can have its governing equations discretized and solved. Meshes that are considered

TABLE 2 Mesh values.

Parameter	Value
Defaults	
Physics preference	CFD
Element order	Program controlled
Element size	3 mm
Sizing	
Growth rate	1.5
Maximum size	Default (10 mm)
Mesh defeaturing and size	Yes, 0.25865 mm
Minimum edge length	0.5 mm
Quality	
Smoothing	Medium
Inflation	Smooth transition
Inflation option	
Transition ratio	0.272
Maximum layers	5
Growth rate	1.2
Statistics	
Nodes	9,468,051
Elements	6,792,615

Abbreviation: CFD, computational fluid dynamics.

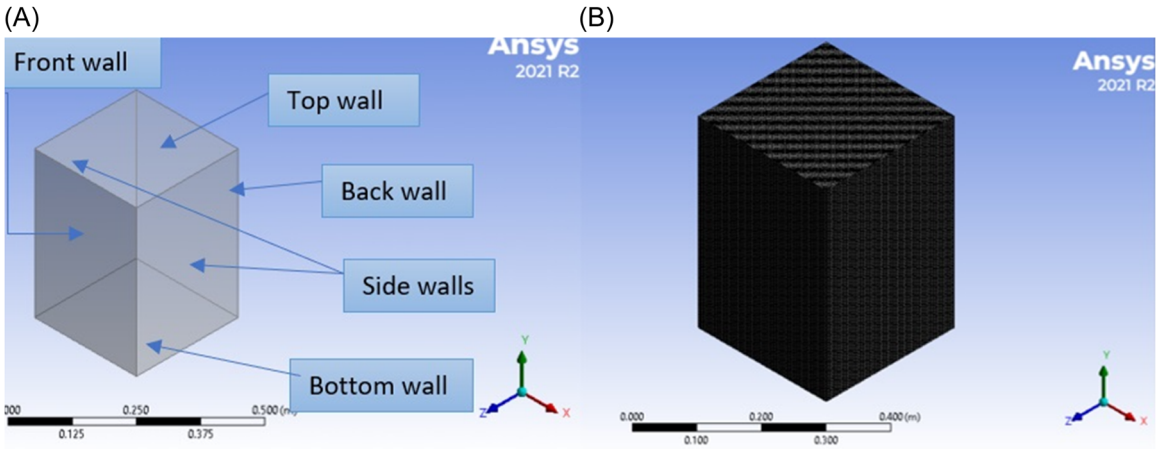

FIGURE 3 (A) Three-dimensional geometry domain. (B) Meshed domain.

acceptable produce outcomes with a reasonable level of accuracy, given that the other model inputs are trustworthy.[63] The primary objective of mesh quality analysis is to correct these errors. To reduce errors with mesh quality, it is essential to understand the standard metrics for mesh quality, regardless of the types of mesh being utilized.

The first main criterion for evaluating a mesh's quality is element quality inspection. The element quality ratio used in this study is 0.83. This indicates that the mesh quality is sufficient to execute a credible simulation. The element quality evaluation provides the composite quality metric, which varies from 0 to 1. A value of 1 denotes a perfect element, whereas an element with a value of 0 has poor element quality.[64] The second main criterion for evaluating a mesh's quality is skewness.[65] The average skewness ratio used in this analysis is 0.229. The meshing quality is ideal if the skewness ratio is between 0 and 0.25 out of the ranges from 0 to 1.[64] When these elements' quality and skewness are within the standard range, it sounds reasonable to trust the results obtained.[66] The mesh's quality ensures the best analysis findings for the problem, reduces the need for extra analysis runs, and increases predictive capabilities. The mesh quality influences the accuracy and convergence of the CFD solution[67] measured by geometric metrics for each cell in the mesh. Extremely skewed computational cells can compromise the solution's stability and accuracy.[68]

2.3.2 | Mesh refinement

A study on mesh refinement has been carried out to investigate the impact of mesh on computation speed and accuracy. The size of the elements significantly affects the problem's convergence and computing time.[69] The structure to be assessed and the extent of the study are the primary determinants of the mesh size selection. It is not possible to obtain adequately accurate results with a high mesh size[70]; while smaller element sizes can lead to a more accurate answer as the design behaves, they also significantly increase calculation time and memory requirements. Both computational time and numerical accuracy are impacted by mesh size. Increased element size causes inconsistent simulation results and convergence issues.

Reducing the size of the elements and analyzing how this affects the correctness of the solution are steps in the mesh convergence process. Less than 10% of the projected element number is considered accurate enough for engineering applications to obtain the ideal element size.[70] Although the processing time increases, the results usually get more precise as the element size lowers. The element number for various element mesh sizes, as determined by ANSYS Fluent, is shown in Figure 4. The element count rises as the element mesh size decreases. The element number does not continue to grow after reaching the optimum value simultaneously. As a result, the value at which precise results were obtained in this study is 0.003 m while considering the lower bound. Furthermore, reducing the mesh size will make the computational system work harder.

2.3.3 | Boundary condition

The cooling cabinet has an internal volume of 0.03 m^3 and is entirely insulated with a 72-mm-thick layer of Po, ensuring optimal thermal efficiency. All walls of the

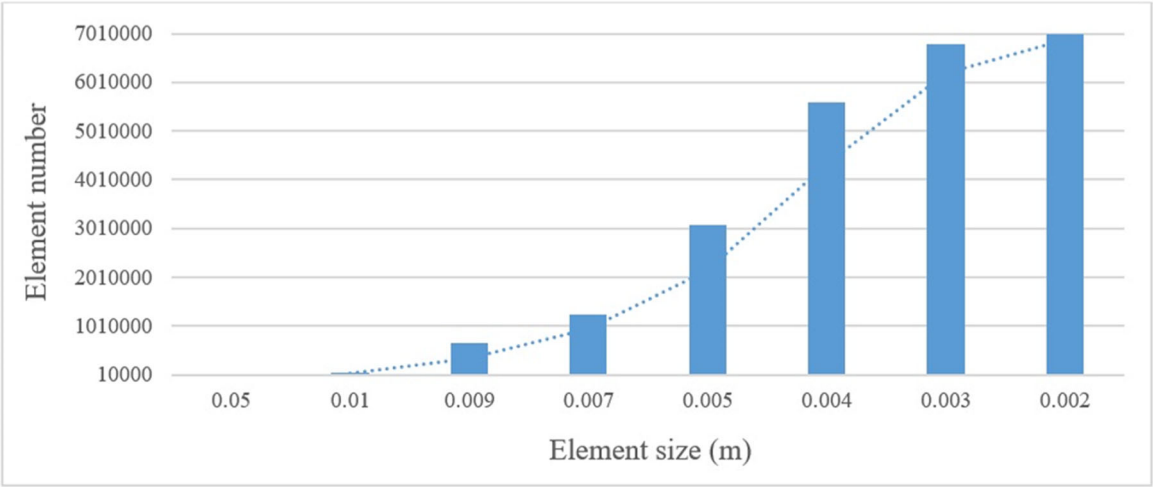

FIGURE 4 Effect of element mesh sizes.

vaccine storage unit were configured as no-slip walls, minimizing heat exchange with the surrounding ambient environments. Figure 5 illustrates the composition of the cabinet's walls, consisting of three material layers. The insulation is achieved through Po sandwiched between an inner aluminum sheet and an outer galvanized sheet serving as the exterior cover. The thickness and thermal conductivity of the insulation materials were carefully incorporated into the analysis. The thermal conductivity values for the insulating materials were sourced from previous studies, as outlined in Table 1. This comprehensive approach allowed for a detailed examination of heat transfer dynamics in different thermal environments.

Table 3 outlines the key characteristics of these materials, emphasizing their role in enhancing the vaccine storage cabinet's insulation and thermal regulation properties. The combination of materials and insulation design plays a crucial role in maintaining stable internal temperatures, safeguarding the stored vaccines from external temperature fluctuations, and ensuring the overall efficiency of the cooling system. By incorporating high-quality insulating materials like Po and a meticulous design approach, the vaccine storage cabinet can effectively uphold the required temperature conditions to preserve vaccine efficacy and safety.

The convective heat coefficients (h) for the walls were calculated based on natural convection using the

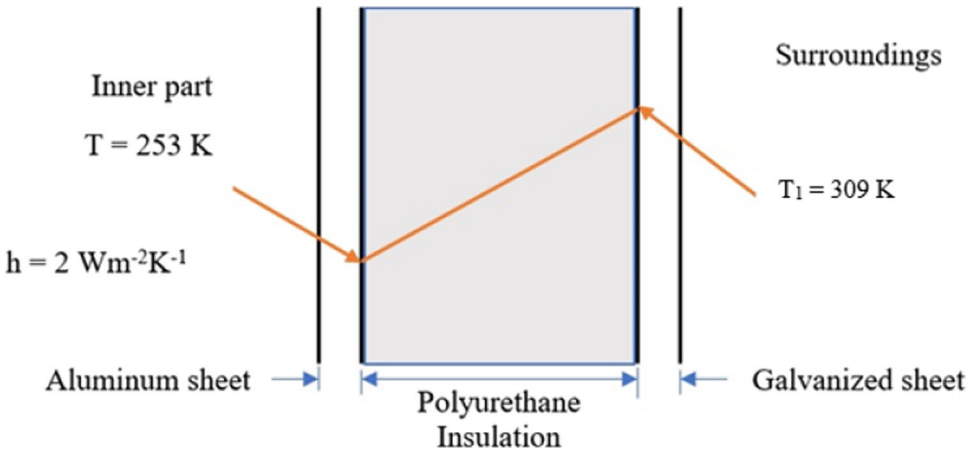

FIGURE 5 Walls of the vaccine storage cabinet.

TABLE 3 Properties and thickness of the wall materials.

Boundary	Condition	ρ (kg m^{-3})	k (W m^{-1} K^{-1})	C_p (J kg^{-1} K^{-1})	x (m)	T_i (K)	h (W m^{-2} K^{-1})
Galvanized sheet	NA	8055	15.1	480	1.5	NA	NA
Polyurethane foam	NA	32	0.0245	1450	72	NA	NA
Aluminum sheet	NA	2702	237	903	1.5	NA	NA
R143a	NA	4.25	0.01409	1425	NA	NA	NA
Top wall	Convective	NA	NA	NA	NA	309	2.2
Front wall	Convective	NA	NA	NA	NA	309	1.8
Side walls	Convective	NA	NA	NA	NA	309	2.4
Back wall	Convective	NA	NA	NA	NA	316	2.0
Bottom wall	Convective	NA	NA	NA	NA	309	2.3
Pressure inflow	Convective	NA	NA	NA	NA	305	NA
Pressure outflow	Convective	NA	NA	NA	NA	253	NA

Abbreviation: NA, not applicable.

dimensionless Nusselt number, Prandtl number, Rayleigh number, and Grashof number[57] (Equations 12–16).

$$h = \frac{Nuk}{L_c}. \tag{12}$$

The heat transfer coefficient by convection is highly dependent on velocity; the higher the velocity, the greater the convection heat transfer coefficient. Natural convection involves low fluid velocities, usually less than $1\ m\ s^{-1}$.[71] As a result, compared to induced convection, natural convection typically has substantially lower heat transfer coefficients. The equations used to calculate *Nu* are:

The front, back, and side walls have been assumed to be vertical plates[57]

$$Nu = \left\{0.825 + \frac{0.387Ra_L{}^{1/6}}{[1 + (0.492/Pr)^{9/16}]^{8/27}}\right\}^2. \tag{13}$$

The top and bottom walls used to be horizontal plate

$$Nu = 0.54Ra_L{}^{1/4}. \tag{14}$$

where

$$Ra_L = Gr_L Pr = \frac{g\beta(T_s - T_\infty)L_c{}^3}{\nu^2}Pr. \tag{15}$$

The top and bottom are considered the characteristic length (L_c) for horizontal walls, while the front, rear, and side are the characteristic length (L_c) for vertical walls.

$$L_c = \frac{A_s}{P_s}. \tag{16}$$

The surface and ambient air temperature were determined using the cabinet walls' values for (T_s) and (T_∞). P_s represents the specific wall's perimeter, while (A_s) represents the wall's surface area.

2.3.4 | Model assumptions

For the boundary condition to be performed, several assumptions were made to simplify the model:

i. The vaccine storage cabinet consists of both fluid and solid domains.
ii. Energy dissipation due to viscosity is negligible.
iii. The temperature difference in the cabinet is due to the density differences.
iv. The flow is laminar, and the airflow within the cabinet is constant.
v. There is no-slip in boundary conditions.

The governing equations considered for the fluid flow and heat transfer include continuity, momentum, and energy equations[57] (Equations 17–19).

i. Continuity equation

$$\nabla.\ \vec{V} = 0. \tag{17}$$

ii. Conservation of momentum

$$u\frac{\partial u}{\partial x} + v\frac{\partial u}{\partial y} = \nu\frac{\partial^2 u}{\partial y^2} + g\beta(T - T_\infty). \tag{18}$$

This equation governs the fluid boundary layer movement due to the effect of buoyancy. Note that the momentum equation involves the temperature; thus, the momentum and energy equations are solved simultaneously.

iii. Conservation of energy

$$u\frac{\partial T}{\partial x} + v\frac{\partial T}{\partial y} = \alpha\frac{\partial^2 T}{\partial y^2}, \tag{19}$$

where the boundary conditions are:

$$\text{At}\quad y = 0: \quad u(x,0) = 0, \quad v(x,0) = 0,$$
$$T(x,0) = T_s$$

$$\text{At}\quad y \longrightarrow \infty: \quad u(x,\infty) \longrightarrow 0, \quad v(x,\infty) \longrightarrow 0,$$
$$T(x,\infty) \longrightarrow T_\infty.$$

2.4 | Simulation temperature validation

The experimental and numerical temperature results from the literature were validated in the current simulation CFD model, as shown in Table 4. The simulation model was conducted by comparing the vaccine storage of 9 L in different locations with different insulation materials. The simulation ran under CFD steady-state analysis at 28°C ambient temperature. In this validation, only the cooling temperature was modeled. The literature temperatures were much higher than those of the simulation CFD model. Nonetheless, the results of the present study reveal a reasonable agreement between the experimental and modeling data. As a result, the model is regarded as validated and suitable for use in the analysis of vaccine storage.

TABLE 4 Comparison of parameters.

Parameters	Literature model[16]	Current model
Model	Vaccine refrigerator	Vaccine cooler
Refrigeration cycle	Vapor compression	Vapor compression
Refrigerant	R134a	R134a
Source of power	Solar	Solar
Size capacity	9 L	30 L
Compressor	12 V, DC	12 V, DC
Condenser	Plate type and finned	Wire and tube
Outer material	Galvanized	Galvanized
Location	Indira Gandhi Institute of Technology	Nelson Mandela Institutions of Science and Technology
Ambient temperature	32°C	28°C
Insulation material	Glass wool	Po
Insulation thickness	32 mm	72 mm

2.5 | Economic feasibility

The significance of comparing the economic feasibility of the designed storage vaccine cooler (DSVC) system with the existing storage vaccine cooler (ESVC) cannot be overstated. This evaluation considers both the initial capital outlay and the yearly operational costs of the entire system. The investment in the storage vaccine cooler includes expenses related to construction, operation, and maintenance. The cost analysis from an economic perspective can be divided into three key categories: capital costs involve the initial investment, encompassing installation expenditures, operating costs account for maintenance and operational charges, and residual and salvage value of the materials.

2.5.1 | Initial investment cost

During the economic analysis process, expenses incurred before a system's operational phase fall under the category of initial investment costs (I_c). These costs play a fundamental role in the overall assessment of economic viability. The initial investment includes acquiring the storage vaccine cooler and procuring materials for its construction. The materials cost (M_c) accounts for the expenses of obtaining the necessary components for the cooler system. Additionally, integrating photovoltaic system costs (PV_c) is part of the initial investment, comprising vital components like solar panels, a charge controller, and a thermostat for temperature regulation. Moreover, labor costs (Lb_c) for constructing and installing these systems are included in the initial investment expenditure. The reliance on solar power in weather conditions highlights the significance of solar battery costs (B_c) during periods with limited sunlight. These costs (Equation 20) significantly influence the project's economic landscape, impacting its long-term sustainability and effectiveness.

$$I_c = M_c + PV_c + Lb_c + B_c. \tag{20}$$

2.5.2 | Operation and maintenance costs

The operation and maintenance costs (OM_c) for both systems encompass manpower and overhead (MOc), including cleaning and leak maintenance, depreciation cost (Dc), and charging of refrigerants (CRc). MOc was assumed to be 3% of the investment cost, covering labor and administrative expenses, as presented by Alrwashdeh and Ammari.[72] D_c was set at 5% of the investment cost, reflecting the system's devaluation. CR_c is assumed to be 3% of the overall operation and maintenance costs, covering refrigerant recharging expenses for system efficiency. Considering these maintenance and operation costs, Equation (21), a more precise economic evaluation can be achieved, offering insights into the long-term financial sustainability of the vaccine cooler system.

$$OM_c = MO_c + D_c + CR_c. \tag{21}$$

2.5.3 | Residual value (salvage value)

The salvage value of the cooler system components (SC_c) is approximated to be approximately 10% of the initial costs, as specified by Wang et al.[73] The salvage value of photovoltaic panels (SP_c) recycling is presumed to be 10% of their total worth. This aspect Equation (22) significantly influences the overall cost-effectiveness and potential returns of the project components.

$$S_v = SC_c + SP_c. \tag{22}$$

2.5.4 | Net present value

When evaluating the economic feasibility of both projects, the net present value method was utilized to determine the equivalent cash flows (C_F) of yearly savings and costs over a specified 10-year period. This assessment incorporates a real discounting rate of 5% to discount future cash flows to their present value. The study utilizes the net present value (NPV) technique to economically compare different cooler system configurations. This method converts the costs and benefits of each option into present value, selecting the option with the highest NPV as the preferred choice among alternatives. The mathematical Equation (23) of NPV value according to Chen et al.[74] was given as

$$\text{net present value} \quad (\text{NPV}) = \sum_{n=1}^{N} \frac{C_F}{(1+i)^n} - I_c. \tag{23}$$

2.5.5 | Payback period

The payback period offers a direct assessment of the time required to recoup an investment, it is crucial to supplement this analysis with other financial metrics for a comprehensive project evaluation. It determines the duration required for an investment to generate adequate cash flows to offset its initial cost. According to De and Ganguly,[75] it is calculated by dividing the capital cost by the average annual net income as Equation (24).

$$P_b = \frac{I_c}{E_s}. \tag{24}$$

2.5.6 | Energy saving

Both systems were assumed to have equal energy savings in providing necessary refrigeration capacity. The annual savings in energy were estimated by taking into account the energy needed to run a standard refrigeration system with specific parameters: a 130 W cooler capacity operating 8 h a day for 365 days. This analysis Equation (25) demonstrates the potential cost savings and environmental advantages of using solar power for refrigeration, emphasizing the efficiency and sustainability of renewable energy sources in industrial settings.[76]

$$E_s = \text{Power}_{\text{compressor}} \times \text{hours}_{\text{day}} \times \text{days}_{\text{year}} \times \text{energy rate}. \tag{25}$$

3 | RESULTS AND DISCUSSIONS

3.1 | Experimental and simulation comparison

The current CFD simulation results were validated using experimental data from a portable vaccine refrigerator with the same model, refrigeration cycle, refrigerant gas, and power source. The comparison of this study's vaccine storage cooler model's simulation results and the experimental results is shown in Figure 6. To validate the simulation results, they were compared with experimental data. This study uniquely demonstrates significantly enhanced cooling performance compared to literature reports, as observed in the studies conducted by Aich and Nayak,[16] Al-Madhhachi and Al-Najideen,[77] and Kherkhar et al.[78] Specifically, while Aich and Nayak[16] reported a cooling temperature of +12°C after 208 min, this study's results displayed a temperature of −12°C after 195 min. Additionally, the average vaccine storage temperature reached +4°C after 124 min in this study's model, whereas the literature model maintained a temperature of 17°C for the same duration. These findings highlight the superior cooling capabilities of this study's model, highlighting substantial improvements over previously reported numerical and experimental results. This suggests that this study's model offers a more effective solution for practical vaccine storage, ensuring the maintenance of required temperatures.

However, statistical analysis revealed deviations ranging from 6.587% for RMSE to 24.2% for MAPE. These differences stem from variations in the type and thickness of insulative materials used in different studies.[24] Addressing this through the standardization of materials and experimental conditions will increase the accuracy of future simulations and reduce errors. In that regard, the uniqueness of this study lies in its comprehensive approach to validating CFD simulation results with experimental data despite potential differences in model size and cycle. While the simulation and experimental setups may not be identical in all aspects, efforts were

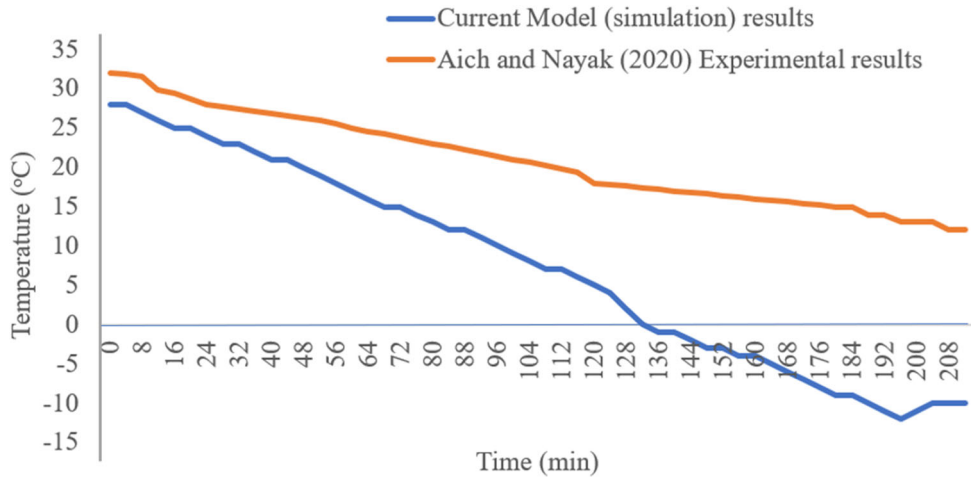

FIGURE 6 Comparison of simulation and experimental results.

made to align critical parameters, such as the model, refrigeration cycle, refrigerant gas, and power source, to ensure meaningful comparison. This thorough validation process, coupled with the significant improvements in cooling performance, distinguishes this study from existing literature and provides a solid foundation for future research and practical applications in vaccine storage solutions.

3.2 | Insulation materials

An essential aspect of designing efficient insulation systems involves utilizing a modeling approach to evaluate transfer processes within insulation materials. A simulation was conducted using conduction and convection thermal modeling with ANSYS Fluent version 2021R2 to analyze the heat transfer rate across a wall, including various surrounding air temperatures (303 and 313 K) for hot climate regions and (278 and 288 K) for cold climate regions aimed to address different climate conditions. Throughout the simulation, the inner temperature remained constant at 253 K. Enhancing insulation performance provides valuable insights into heat flow and energy transfer, ultimately improving cooling efficiency for vaccine storage purposes.

Figures 7 and 8 present the results of a CFD simulation analyzing the insulating heat transfer and external wall temperature properties of cold and hot regions at temperatures of 278, 288, 303, and 313 K. The simulation outcomes reveal that, among the tested insulating materials, Po scored 20.2%, Fe scored 20.1%, Fl scored 20.0%, Fi scored 19.6%, and Co scored 18.9% in terms of insulating wall performance. In contrast, the insulative heat transfer results indicated that Po scored 14.3%, Fe scored 18.7%, Fl scored 19.8%, Fi scored 21.9%, and Co scored 25.3%. The data illustrate that Po outperforms other insulation materials regarding heat transfer and demonstrates greater resistance to external temperature impacts on the cooling cabinet at both cold and hot region climate conditions. Across various reference temperatures, Po exhibits the lowest heat transfer rate, with Fe following closely behind. Utilizing highly efficient thermal insulation materials and advanced insulation techniques can extend insulation duration and enhance energy efficiency significantly.[79] Selecting an insulating material with superior insulative qualities, such as Po, is crucial for optimizing insulation effectiveness and maintaining stable internal temperatures within the storage system.

It is evidence that the thermal conductivity factor plays a critical role in determining the most suitable insulating material for the cooling process. In this context, the best two alternative insulative materials that scored the highest grade in wall performance can be used for the vaccine coolers such as Fe and Fl because their difference is 0.1% and 0.2%, respectively. The practicality of these insulative materials is highly commendable, given their widespread availability in various sizes and volumes within the local market. Equipped with this insulation, the cooler's ability to function effectively in various climate and environmental conditions presents it as a promising solution for facilities that are hard to access and suffer from unstable power sources.

Notably, Po exhibits low moisture-vapor permeability, strong low density, considerable mechanical strength, and resistance to water absorption, making it an excellent choice for thermal insulation purposes, as highlighted by Gama et al.[80] Furthermore, the installation of Po is relatively straightforward and cost-effective, adding to its appeal as a preferred

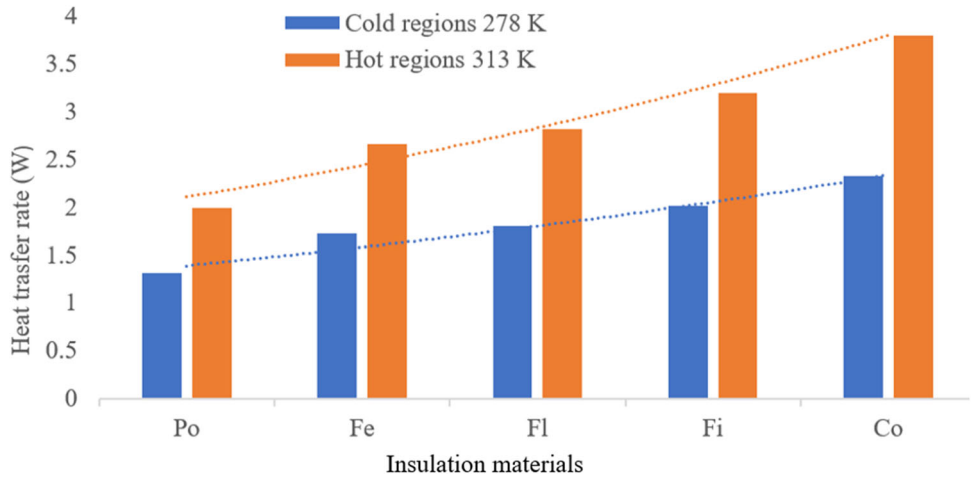

FIGURE 7 Insulating materials in different heat transfer rates.

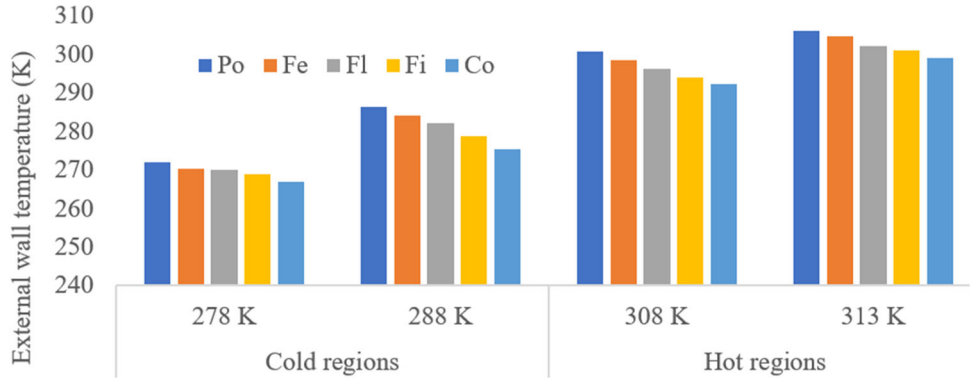

FIGURE 8 Insulating materials in different climate regions.

insulating material for applications requiring efficient temperature regulation and thermal insulation.[81] The versatility, effectiveness, and practicality of Po position it as a reliable and efficient solution for enhancing thermal insulation in the context of the cooling process, underscoring its value as a critical component in maintaining optimal conditions within the vaccine storage system.

3.3 | Effects of insulation thickness

Figure 9 presents a CFD simulation focusing on the insulation thickness within the vaccine storage cabinet. The simulation results indicate that an insulation thickness of less than 0.06 m resulted in poor insulation performance, leading to increased heat transfer within the cabinet. Conversely, the simulation demonstrates that an insulation thickness of 0.07 m performs more effectively, serving as the baseline for the analysis. Consequently, this study adopts an insulation thickness of 0.072 m to enhance the cooling medium's ability to maintain the desired temperature within the cabinet over an extended period. The selection of the optimal thickness was based on considerations such as design requirements and available space for accommodating the condenser on the outer cover.

In Figure 9A, heat transfer from the interior to the outer wall of the cabinet is observed when the insulation thickness is below 0.06 m, highlighting the inefficiency of inadequate insulation. In contrast, Figure 9B illustrates the absence of heat penetration due to the presence of thicker insulation exceeding 0.07 m. The insulation thickness and the choice of materials utilized directly influence the effectiveness of maintaining cooling within the cabinet. Generally, a thicker insulation layer correlates with enhanced cooler performance, while thinner insulation may compromise efficiency. The insulation thickness serves as a critical factor governing heat exchange with the surrounding environment, underscoring the importance of selecting an appropriate thickness to optimize the cooler's overall performance and ensure efficient temperature regulation within the vaccine storage system.

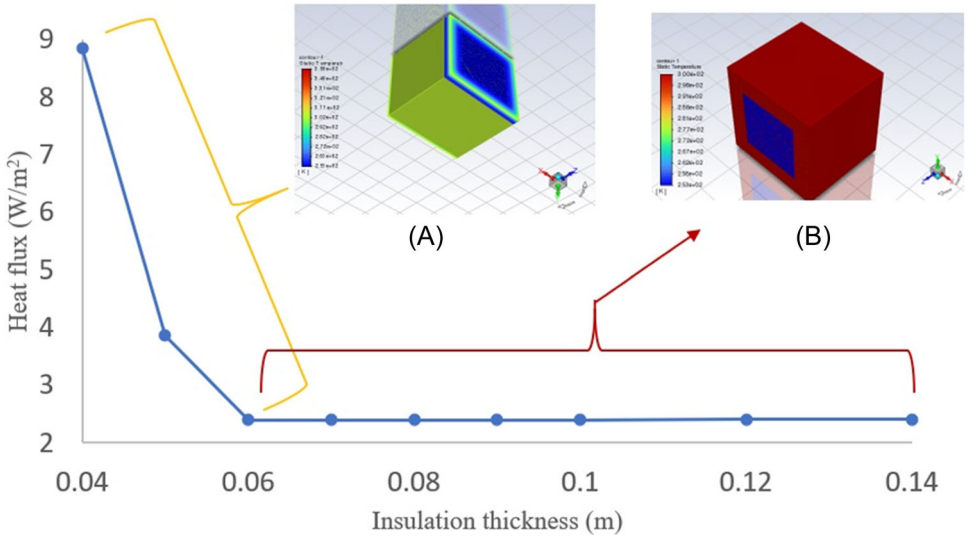

FIGURE 9 Heat flux against insulation thickness (A–B).

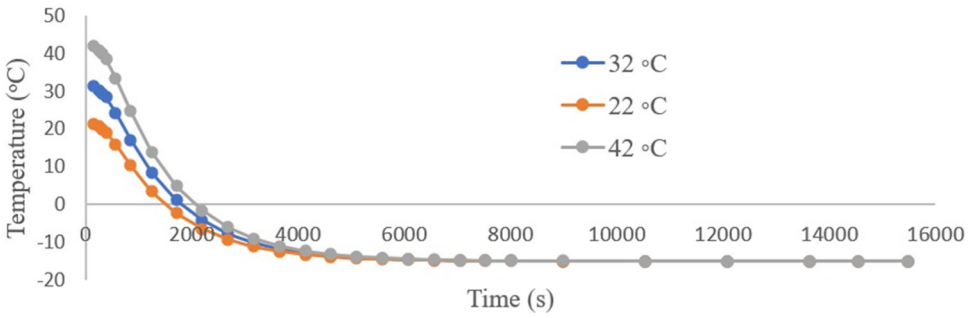

FIGURE 10 Effects of ambient temperature.

3.4 | Effects of ambient temperature

In Figure 10, the influence of ambient temperatures on the cooling system is depicted. As the ambient temperature escalates to 42°C, the temperature differential diminishes, reducing the condenser's efficiency and cooling power. The findings reveal that the effectiveness of cooling diminishes as the ambient temperature rises, with the lowest ambient temperature yielding optimal cooling performance. Conversely, higher ambient temperatures result in reduced cooling efficiency. Despite these variations, all ambient temperatures converge at −15°C and remain constant throughout the operational cycle, contingent on the heat source powering the compressor. Precisely, the ambient temperature of 22°C aligns with the −15°C mark after 4740 s, while the ambient temperatures of 32°C and 42°C reach this equilibrium after 5580 and 6540 s, respectively, reflecting a deviation of 14.67%. This deviation underscores the impact of ambient temperatures on the cooling process. It highlights the critical role of maintaining optimal environmental conditions to ensure efficient cooling performance and temperature regulation within the vaccine storage system.

The fluctuation in ambient temperature significantly influences the cooling performance of vaccine storage systems. Descriptive statistical analyses conducted by Mupangwa et al.[82] highlight the wide range of temperatures experienced in Sub-Saharan Africa, with maximum temperatures reaching up to 43°C and minimums dropping below 20°C in various regions. This study considers the minimum, average, and maximum temperatures in Sub-Saharan Africa to be 22°C, 32°C, and 42°C, respectively.[83] It is noted that as the temperature of the evaporator increases, the efficiency of the cooling device decreases.[84] Despite the challenges posed by high ambient temperatures, the cooling storage system demonstrates the capability to effectively extract a substantial amount of heat flux from electronic components, ensuring that their temperature remains below the critical

limit of 42°C. This resilience in cooling efficiency under varying ambient conditions underscores the system's ability to maintain optimal temperatures for vaccine storage, even in environments with elevated ambient temperatures, thereby safeguarding the integrity and efficacy of the stored vaccines.

3.5 | Temperature distribution within the cabinet

Figure 11 provides insight into the temperature distribution within the cabinet. The model incorporates evaporator coils located on the vertical sides of the

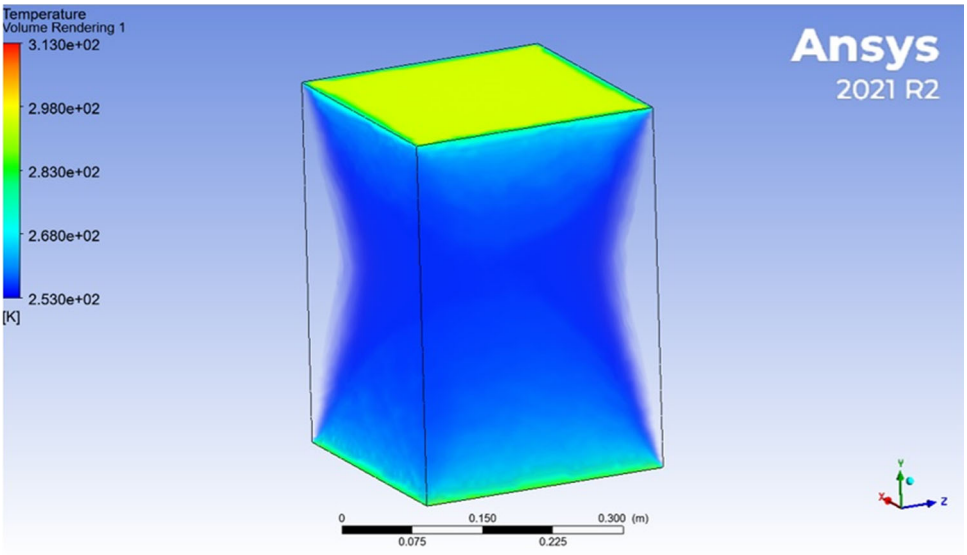

FIGURE 11 Temperature volume rendering.

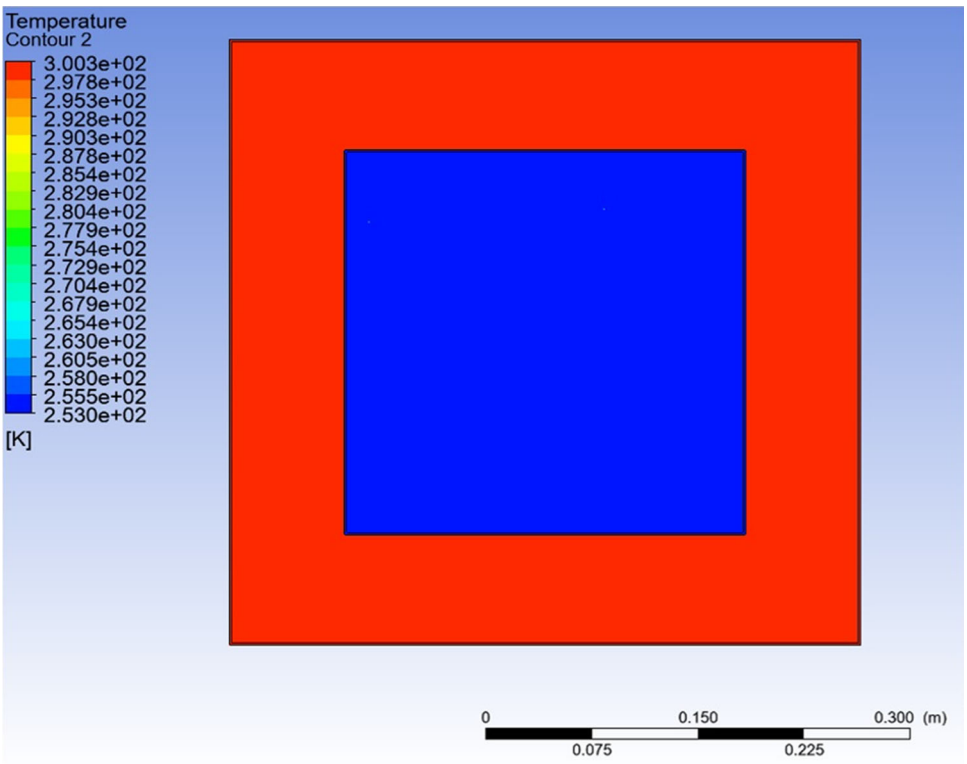

FIGURE 12 Temperature distribution in the cabinet.

vaccine storage unit. These coils facilitate cooling within the cabinet through the vertical sides, resulting in temperature variations between the vertical sides and the top and bottom sections. The vertical sides achieve a lower temperature of 253 K, effectively cooling the cabinet, while the uncovered top side reaches up to 313 K when ambient temperatures are high. By integrating proper insulation materials, the storage vaccine can maintain the required temperature and prevent the rapid loss of coldness. The simulation outcomes demonstrate that with adequate insulation, the model can achieve a temperature of 253 K, meeting the ultra-low temperature standards necessary for vaccine storage in remote areas. The system exhibits efficient natural convection, a characteristic favored in smaller coolers, as highlighted by Logeshwaran and Chandrasekaran.[85] In contrast, forced convection is noted to offer enhanced temperature uniformity in larger cooling systems. The strategic placement of evaporator coils and the utilization of insulation materials play a vital role in maintaining optimal temperatures for vaccine storage, particularly in challenging environments where consistent cooling is essential.

In Figure 12, the temperature distribution within the cabinet is illustrated. The reddish color represents the

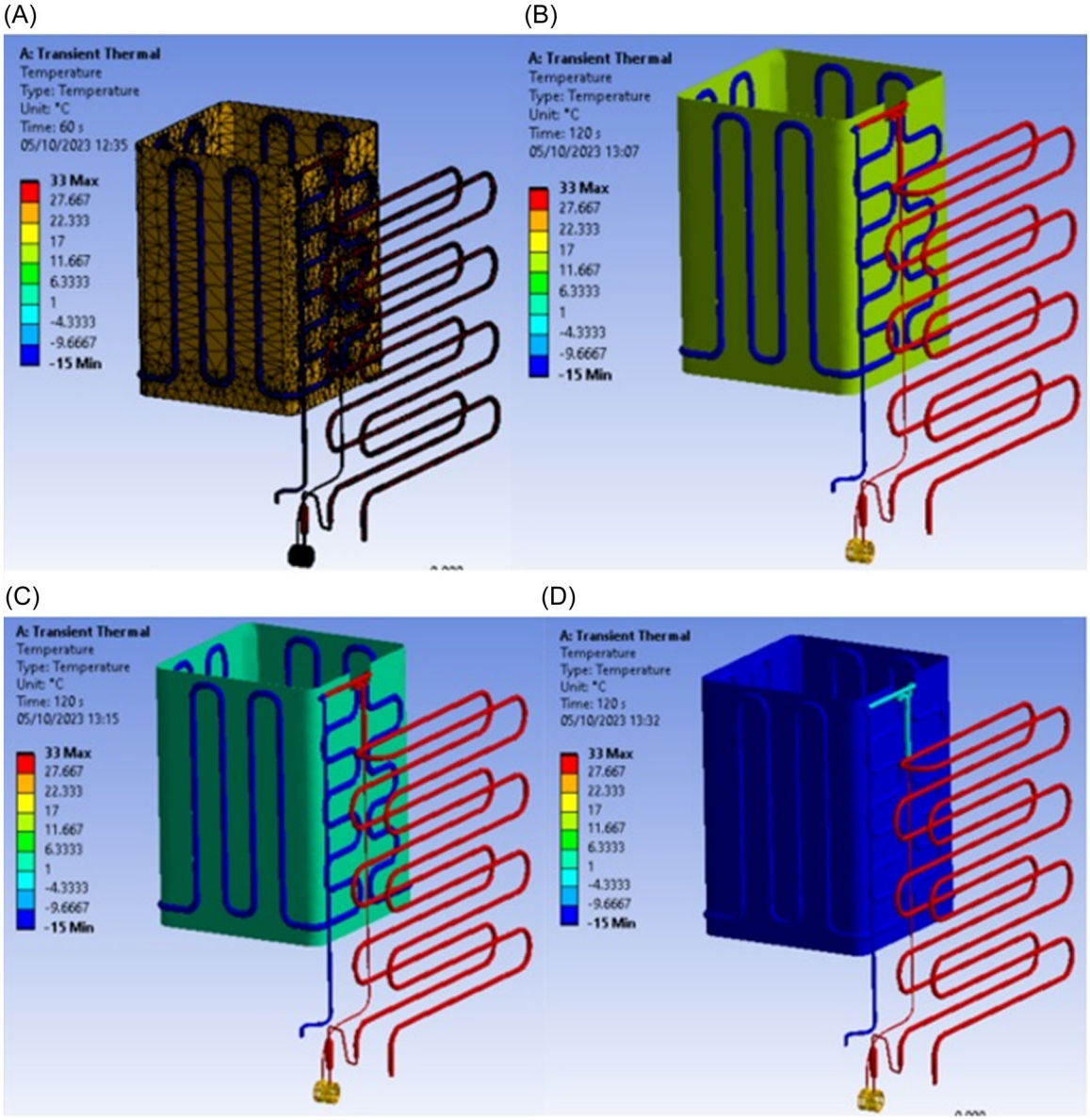

FIGURE 13 Temperature distribution within refrigeration systems. (A–D) The temperature variations within the refrigerant flow. (A) The temperature at 26 degree Celsius during the initial stage of compressing. (B) The refrigerant flow at the condenser stage. (C) The refrigerant flow at the capillary tube stage. (D) The refrigerant flow at the evaporator stage.

outer temperature in the surroundings, maintained at approximately 300 K on the outer layer of the cooler. In contrast, the bluish color signifies the minimum temperature inside the cabinet, measuring around 253 K, a crucial temperature requirement based on the specific type of vaccine stored at any given time. The bluish cooler area indicates the minimum temperature necessary for the effective cooling of the vaccines. The simulation results reveal that the inside compartment reaches 253 K, while the outer cover attains 300 K at the galvanized sheet. These temperature settings were established as the boundary conditions range during the vaccine

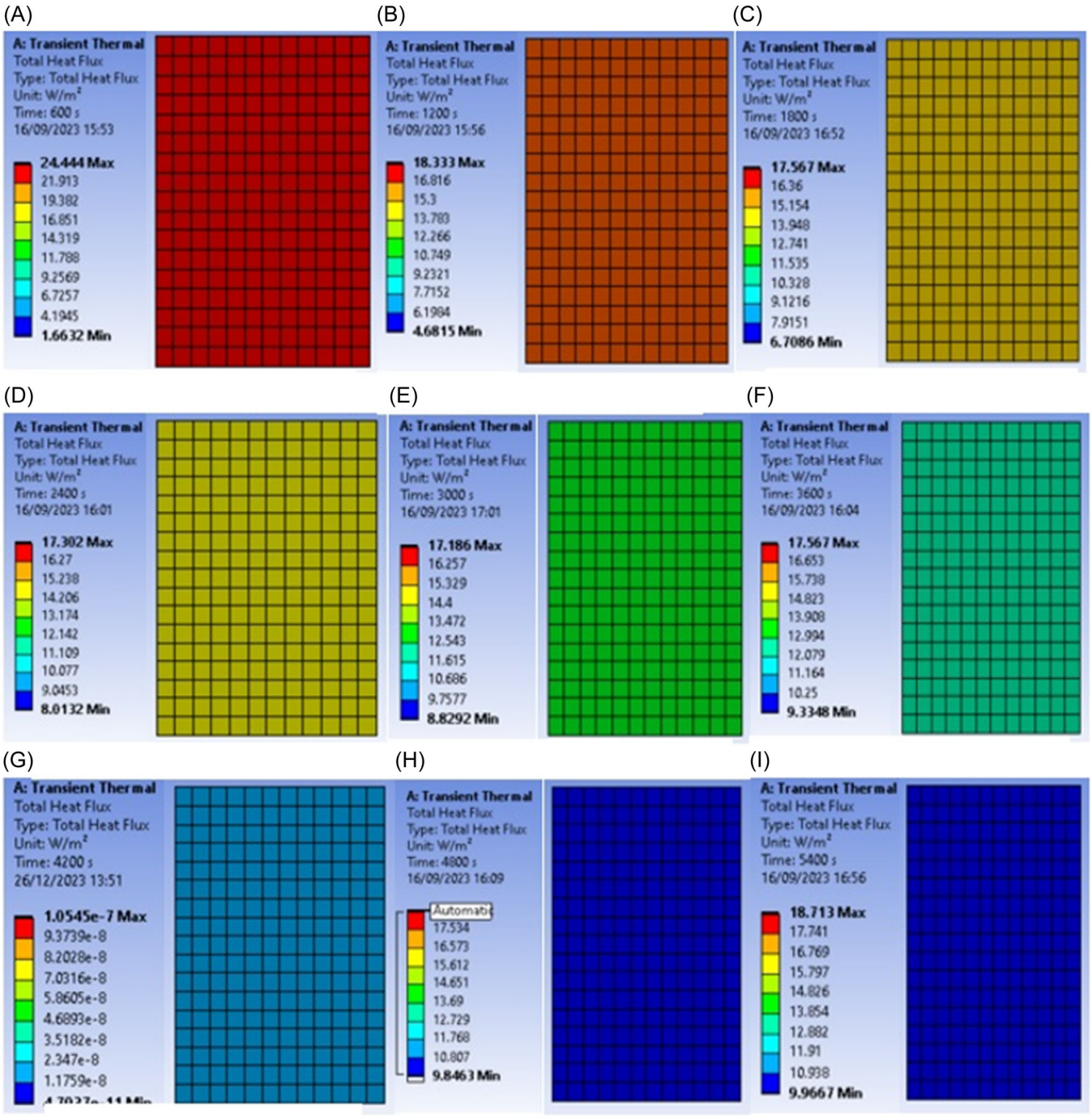

FIGURE 14 Heat flux variation in temperature cabinet wall. (A–I) Wall temperature variations within the vaccine cooler cabinet, through heat fluxes. This was Computational Fluid Dynamics (CFD) simulation conducted through transient thermal analysis. However, (A) indicates the measured temperature after 10 minutes, (B) temperature measured after 20 minutes, (C) temperature measured after 30 minutes, (D) temperature measured after 40 minutes, (E) temperature measured after 50 minutes, (F) temperature measured after 60, (G) the temperature measured after 70, (H) the temperature measured after 80 minutes, and (I) temperature measured after 80 minutes.

storage simulation to adhere to the designated temperature of 258 K required for optimal storage conditions in this study. By maintaining a temperature range between 253 and 281 K within the cabinet, the system ensures that the vaccines are stored at the appropriate temperature levels to preserve their efficacy. The color representation provides a visual depiction of the temperature distribution, highlighting the contrast between the outer and inner temperatures within the vaccine storage unit to maintain the desired conditions for the safe and effective storage of vaccines.

3.6 | Temperature distribution within the refrigeration systems

Figure 13 showcases the static temperature contours of refrigeration systems, comprising essential components such as the compressor, condenser, capillary tube, and evaporator that collectively form the vapor compression cooling system. Operating at an ambient temperature of 26°C, the compressor plays a pivotal role in compressing the refrigerant and directing it to the condenser. As the compressor functions to elevate

TABLE 5 Financial analysis of the two refrigeration technologies.

	DSVC cost analysis		ESVC cost analysis	
Types of cost	**Value ($)**	**Total ($)**	**Value ($)**	**Total ($)**
Investment cost, $			1250	
Manufacturing materials cost	402			
Purchase 200 W solar panel costs	350			
Purchase solar battery 150AH costs	250			
DC Compressor cost	145			
Insulation materials cost	63			
Evaporator cost	13			
Condenser cost	21			
Wiring equipment cost	25			
Purchase R134a refrigerant	15			
Capillary tube cost	8			
Labor charge costs	85			
		1377		1250
Operation & maintenance cost, $ per year				
Manpower and overhead costs, 3% of investment cost	41.3		37.5	
Depreciation 5% investment cost	68.9		62.5	
Charge of leaks of refrigerant cost 3% OMc	3.3		3	
		113.5		103
Residual value at the 10th year, $				
Residual value 10% of the initial costs	137.7		125	
The salvage value of PV modules is 10% of the total value	35		0	
		172.7		125
Energy saving, $ per year	94.9		94.9	
		94.9		94.9

both pressure and temperature,[86] the coils of the condenser transition to a reddish hue, indicating a temperature rise. The condenser receives the hot, high-pressure refrigerant and utilizes ambient air to facilitate cooling, bringing the refrigerant to its saturation temperature before condensing it into a liquid state entirely.[87] Subsequently, the refrigerant passes through the capillary tube, where a pressure drop occurs, causing some vaporization of the high-pressure liquid due to decreased temperatures. This process leads to the generation of low-temperature liquid that effectively induces cooling within the evaporator component. The evaporator coils, depicted in blue color, represent the cooling effects within the cabinet, highlighting the functionality of the refrigeration system in maintaining optimal temperatures for the storage of vaccines. The color variations in the static temperature contours offer a visual representation of the refrigeration system's operation and its role in ensuring efficient cooling within the designated storage environment.

Subsequently, the refrigerant within the evaporator persistently emits coldness into the cabinet through natural convection, facilitated by the coil integrated into the vertical sides of the wall. This cooling mechanism progresses in the liquid phase, gradually reducing the temperature within the cabinet from the initial 26°C (depicted in Figure 13A) to the ultimate minimum temperature of −15°C (illustrated in Figure 13D). The transition from higher temperatures in the evaporator coils to lower temperatures continues as long as the compressor remains operational. The sequence of Figure 13A–D represents the temperature variations occurring within the evaporator and compressor coils, showcasing the dynamic cooling process and temperature adjustments essential for maintaining optimal conditions within the refrigeration system.

3.7 | Heat flux variation in temperature cabinet wall

Figure 14 presents the heat flux variation in the temperature cabinet wall. By conducting a transient thermal analysis using CFD, the walls of the vaccine storage cabinet were assessed to determine the distribution of heat flux over time. The findings indicate that the heat flux decreased to −15°C after 76 min at an ambient temperature of 22°C, observed between Figure 14G and Figure 14H. The reduction in heat flux signifies the transfer of heat from the warmer areas to the cooler regions.[88] A minor inconsistency of 3.7% is noted between the heat flux concentration and the impact of the ambient temperature, attributed to the varied time steps in transient and steady-state analyses. Despite this slight deviation, it does not affect the overall validity of the results obtained. Instead, it provides robust evidence supporting the accuracy of the findings. The comparison of heat flux variations over time offers valuable insights into the heat transfer dynamics within the vaccine storage cabinet, emphasizing the critical role of transient thermal analysis in assessing temperature fluctuations and ensuring the efficient preservation of vaccines at the required low temperatures.

3.8 | Economic analysis

The economic feasibility of the storage vaccine coolers was meticulously assessed through a comparison between the DSVC and the ESVC. This assessment focused on crucial factors such as the initial investment costs, operational and maintenance costs, and residual and salvage value of material components, as detailed in Table 5. The DSVC reflected an investment cost of $1377, slightly higher than the $1250 for the ESVC. This cost disparity can be attributed to the prototype stage of the designed cooler, despite utilizing local materials. Furthermore, the operation and maintenance costs of the DSVC were notably higher, primarily due to a percentage increase linked to the initial investment cost. In contrast,

TABLE 6 Profitability measure for net present value.

Year	Discount rate (5%)	Net cash flow		Present value ($)	
		DSVC	ESVC	DSVC	ESVC
1	0.952380952	267.6	219.9	254.8571	209.4286
2	0.907029478	267.6	219.9	242.7211	199.4558
3	0.863837599	267.6	219.9	231.1629	189.9579
4	0.822702475	267.6	219.9	220.1552	180.9123
5	0.783526166	267.6	219.9	209.6716	172.2974
6	0.746215397	267.6	219.9	199.6872	164.0928
7	0.71068133	267.6	219.9	190.1783	156.2788
8	0.676839362	267.6	219.9	181.1222	148.837
9	0.644608916	267.6	219.9	172.4973	141.7495
10	0.613913254	267.6	219.9	164.2832	134.9995
Cumulative present value ($)				2066.336	1698.01
Net present value ($)				689.336	448.01
Rate of return on investment (%)				19.43	17.59
Payback period (year)				5.1	5.6

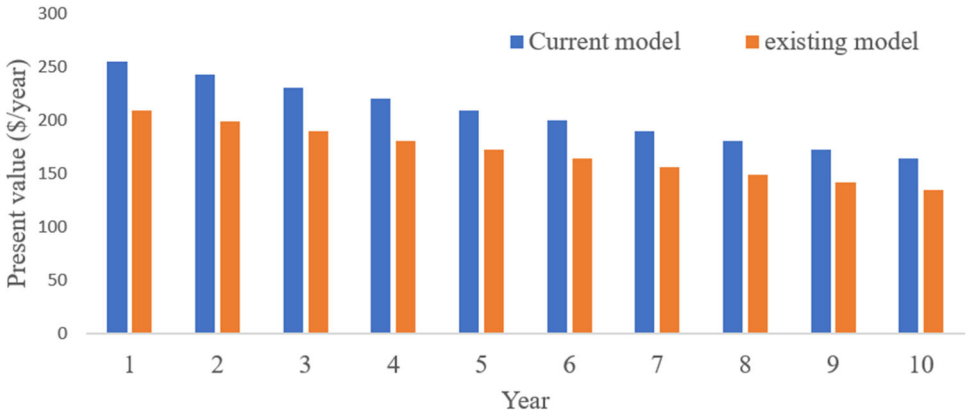

FIGURE 15 Comparison of present value for coolers.

the ESVC experienced a decrease in residual and salvage value, stemming from the absence of salvageable components. Based on profitability analysis, Table 6 presents key metrics such as annual net cash flow, present value, net present value, payback period, and return on investment. The net present value for the DSVC stood at $689.336, while the ESVC yielded $448.01. Notably, the return on investment and payback period were calculated at 19.43% (5.1 years) and 17.59% (5.6 years), respectively, for the DSVC and ESVC. In conclusion, both storage vaccine coolers demonstrated economic viability based on the calculated parameters and underlying assumptions. However, the DSVC, as shown in Figure 15, emerged as the more profitable option, given its higher net present value. This signifies its attractiveness as an investment with promising returns, making it a compelling choice for vaccine cooling solutions.

4 | CONCLUSION AND RECOMMENDATION

A solar-powered cooler for vaccine storage is designed and tested through CFD simulation at different temperatures of 313, 275, and 253 K. Moreover, it reveals that it can work and successfully operate in the local climatic conditions in sub-Saharan Africa. Furthermore, the CFD simulation for the insulating wall of the vaccine storage shows that the Po scores 0.49% more than other insulation materials. The practicability and availability of the Po material found at the local market guarantee the selection in this study. The insulation thickness of 72 mm was accepted according to the design structure. The evaporator coils rotate at both sides of the vertical wall, which is very effective in natural convection. Similarly, natural convection signifies the cabinet's effectiveness through temperature distribution within the cabinet and volume rendering analysis.

A 3D CFD model was developed for vaccine storage to validate the cooling time within the cabinet and heat transfer rate through different ambient temperatures. On this remark, the present simulation shows good results compared with the experimental and numerical results. It takes 33.3% less than the reported experimental and numerical cooling duration results. Furthermore, the experiment and numerical results deviate by 6.587% and 24.2% when using statistical analyzing of RMSE and mean average percentage error, respectively, from the current results. The ultralow temperature of −12°C was reached with a COP of 4.5.

The economic analysis conducted revealed a payback period of 5.1 and 5.6 years for the DSVC and the ESVC respectively. The results of cost analysis have indicated that both complete systems are cost-effective regarding their benefits over their total costs. Additionally, the present model can be considered as an agreement to fulfill the requirements of the methodology and favor the current vaccine storage for improving cooling performance. On the other hand, this is due to the proper insulative material used in the vaccine storage. However, further research is needed on CFD to integrate solar and other renewable energy to effectively enhance vaccine storage in remote areas during the rainy season and other complications of sunshine and improve the simulation of the leakage of the vaccine storage for betterment and effectiveness of the vaccine storage technology.

NOMENCLATURE

3D	three dimension
A_s	surface area (m^2)
A_w	surface area of the wall (m^2)
B_c	batteries costs ($)
C_F	Cash flow ($)
Co	coconut fiber

C_p	specific heat capacity ($J\,kg^{-1}\,K^{-1}$)
CR_c	charging of refrigerants ($)
E_s	Energy saving ($)
Fe	feather fiber
Fi	fiberglass
Fl	fly ash
g	acceleration due to gravity ($m\,s^{-2}$)
Gr	Grashof number
h	convective heat coefficients ($W\,m^{-2}\,K^{-1}$)
h_i	heat transfer coefficients at the inner
h_o	heat transfer Coefficients at the outer
I_c	initial investment costs ($)
K	Kelvin (K)
k_A	thermal conductivity of galvanized sheet ($Wm^{-1}K^{-1}$)
k_B	thermal conductivity of aluminum sheet ($W\,m^{-1}\,K^{-1}$)
k_C	thermal conductivity of polyurethane foam ($W\,m^{-1}\,K^{-1}$)
L_b	labor costs ($)
L_c	characteristic length (m)
M_c	materials costs ($)
MO_c	manpower and overhead costs ($)
Nu	Nusselt number
N/A	not applicable
OM_c	operation and maintenance costs ($)
P_b	Payback period (years)
Po	polyurethane foam
Pr	Prandtl number
P_s	perimeter (m)
PV_c	Photovoltaic system costs ($)
Q_E	evaporator load (W)
Q_L	condenser load (W)
Q_P	compressor power (W)
Ra	Rayleigh number
SC_c	salvage of system components costs ($)
SP_c	Salvage of photovoltaic panel costs ($)
T_i	inner temperature (K)
T_s	surface temperature (K)
T_∞	ambient temperature (K)
V	voltage (V)
W	watts (W)
W_C	work done by compressor ($kJ\,kg^{-1}$)
X	thickness (m)
x_A	thickness of aluminum sheet
x_B	thickness of galvanized sheet
x_C	thickness of polyurethane foam
ρ	density ($kg\,m^{-3}$)
β	coefficient of expansion (K^{-1})
υ	kinematic viscosity ($m^2\,s^{-1}$)
°C	degree Celsius
$\dot{m}$	mass flow rate ($kg\,s^{-1}$)

AUTHOR CONTRIBUTIONS

Vicent Marwa, Thomas Kivevele, Baraka Kichonge, and Juma Selemani were involved in the conceptualization, methodology, validation, and formal analysis; Vicent Marwa wrote the article, original draft, and visualization, and Thomas Kivevele, Baraka Kichonge, and Juma Selemani revised for intellectual content, supervision, review, and editing; and all the authors gave their approval to the submitted version.

ACKNOWLEDGMENTS

The authors would like to thank the SOVAS PROJECT through The Nelson Mandela African Institute of Science and Technology and the HEET PROJECT through the Mbeya University of Science and Technology for financial support in this work.

CONFLICT OF INTEREST STATEMENT

The authors declare no conflict of interest.

ORCID

Vicent Marwa http://orcid.org/0009-0008-2679-1863
Thomas Kivevele http://orcid.org/0000-0003-4539-6021

REFERENCES

1. Gilano G, Sako S, Molla B, Dekker A, Fijten R. The effect of mHealth on childhood vaccination in Africa: a systematic review and meta-analysis. *PLoS One*. 2024;19:0294442. doi:10.1371/journal.pone.0294442
2. USAID. New Report Reflects on United States' Historic Effort to Accelerate COVID-19 Vaccine Delivery, Demand, and Uptake Globally| Press Release | U.S. Agency for International Development. 2023. https://www.usaid.gov/news-information/press-releases/sep-14-2023-new-report-reflects-united-states-historic-effort-accelerate-covid-19-vaccine-delivery-demand-and-uptake-globally
3. Makhijani S, Elossaily GM, Rojekar S, Ingle RG. mRNA-based vaccines—global approach, challenges, and could be a promising wayout for future pandemics. *Pharm Dev Technol*. 2024;29:559-565. doi:10.1080/10837450.2024.2361656
4. Abbasi S, Zahmatkesh S, Bokhari A, Hajiaghaei-Keshteli M. Designing a vaccine supply chain network considering environmental aspects. *J Clean Prod*. 2023;417:137935. doi:10.1016/J.JCLEPRO.2023.137935
5. Lewis LM, Badkar AV, Cirelli D, Combs R, Lerch TF. The race to develop the Pfizer-BioNTech COVID-19 vaccine: from the pharmaceutical scientists' perspective. *J Pharm Sci*. 2023;112:640-647. doi:10.1016/j.xphs.2022.09.014
6. Santos AF, Gaspar PD, de Souza H. Refrigeration of COVID-19 vaccines: ideal storage characteristics, energy efficiency and environmental impacts of various vaccine options. 2021.
7. CDC. *Vaccine Storage and Handling Toolkit-Updated with COVID-19 Vaccine Storage and Handling Information*. April 2022. www.cdc.gov/vaccines/imz-managers/awardee-imz-websites.html

8. Osho Z, Sareen J. Accessing solar energy to deliver healthcare for all. *Resilient Health*. 2024:301-309. doi:10.1016/B978-0-443-18529-8.00024-X
9. Pangaribowo EH, Iskandar DD. Exploring socio-economic determinants of energy choices for cooking: the case of eastern Indonesian households. *Environ Dev Sustain*. 2022:1-14. doi:10.1007/S10668-022-02362-Y
10. Röder M, Chong K, Thornley P. The future of residue-based bioenergy for industrial use in Sub-Saharan Africa. *Biomass Bioenergy*. 2022;159:106385. doi:10.1016/J.BIOMBIOE.2022.106385
11. Lennon P, Atuhaire B, Yavari S, et al. Root cause analysis underscores the importance of understanding, addressing, and communicating cold chain equipment failures to improve equipment performance. *Vaccine*. 2017;35(17):2198-2202. doi:10.1016/j.vaccine.2016.09.068
12. Kumar S, Lennon P, Uranw S, et al. Using freeze-preventive cold boxes in rural Nepal: a study of equipment performance, acceptability, system fit, and cost. *Vaccine X*. 2024;18:100467. doi:10.1016/j.jvacx.2024.100467
13. Bayraktar FS, Kose R, Phase Change Materials: types, Properties and Applications in Buildings. *Bayraktar&Köse/Kırklareli Univ J Eng Sci*. 2022;8(1):190-210. doi:10.34186/klujes.1126167
14. Geng L, Huang W, Jiang J, et al. Cold energy storage enhancement and phase transition temperature regulation. *J Energy Storage*. 2024;97:112903. doi:10.1016/J.EST.2024.112903
15. Li M, Xie B, Li Y, Cao P, Leng G, Li C. Emerging phase change cold storage technology for fresh products cold chain logistics. *Journal of Energy Storage*. 2024;88:111531. doi:10.1016/J.EST.2024.111531
16. Aich S, Nayak J (2020). Design and fabrication of a solar portable refrigerator. *Mater Today Proc*. doi:10.1016/j.matpr.2020.08.442
17. Ray AK, Singh S, Rakshit D. Comparative study of cooling performance for portable cold storage box using phase change medium solid-liquid latent heat energy stored (J) temperature (K). *Therm Sci Eng Progr*. 2022;27:101146. doi:10.1016/j.tsep.2021.101146
18. Zhang M, Sun J, Fricke B, et al. A study on computational fluid dynamics modeling of a refrigerated container for COVID-19 vaccine distribution with experimental validation. *Int Commun Heat Mass Transfer*. 2022;130:105749. doi:10.1016/j.icheatmasstransfer.2021.105749
19. Ng CZ, Lean YL, Yeoh SF, et al. Cold chain time- and temperature-controlled transport of vaccines: a simulated experimental study. *Clin Exp Vaccine Res*. 2020;9(1):8-14.
20. Luerssen C, Sekhar C, Cheong D, Reindl T. Solar-powered cooling for the remote tropics. *Green Energy Technol*. 2020:31-62. doi:10.1007/978-3-030-41952-3_3
21. Ben Taher MA, Kousksou T, Zeraouli Y, Ahachad M, Mahdaoui M. Thermal performance investigation of door opening and closing processes in a refrigerated truck equipped with different phase change materials. *J Energy Storage*. 2021;42:103097. doi:10.1016/j.est.2021.103097
22. Söylemez E, Alpman E, Onat A, Yükselentürk Y. CFD analysis for predicting cooling time of a domestic refrigerator with thermoelectric cooling system Analyse CFD pour la prévision de la durée de refroidissement d' un réfrigérateur domestique avec système de refroidissement thermoélectrique. *Int J Refrig*. 2021;123:138-149. doi:10.1016/j.ijrefrig.2020.11.012
23. Chen M, Zhao J, Zhang Z, Gu C, Wang X. Influencing factors of thermal performance of small-size vaccine cold storage: an experiment-based parametric study. *J Energy Storage*. 2022;51:104496. doi:10.1016/J.EST.2022.104496
24. Leungtongkum T, Flick D, Hoang HM, Steven D, Delahaye A, Laguerre O. Insulated box and refrigerated equipment with PCM for food preservation: state of the art. *J Food Eng*. 2022;317:110874. doi:10.1016/J.JFOODENG.2021.110874
25. Kumar VV. Investigation of the thermal performance of coconut fibre composite with aluminium reflector cooling roofs. *Environ Dev Sustain*. 2018;22:0123456789. doi:10.1007/s10668-018-0285-x
26. Pavithra KS, Parol V, Solomon AB, Yashoda MP. Investigation of thermal conductivity and thermal performance of heat pipes by structurally designed copolymer stabilized ZnO nanofluid. *Sci Rep*. 2023;13:14219. doi:10.1038/s41598-023-39598-1
27. Massoudinejad M, Amanidaz N, Santos RM, Bakhshoodeh R. Use of municipal, agricultural, industrial, construction and demolition waste in thermal and sound building insulation materials: a review article. *J Environ Health Sci Eng*. 2019;17:1227-1242.
28. Dieckmann E, Onsiong R, Nagy B, Sheldrick L, Cheeseman C. Valorization of waste feathers in the production of new thermal insulation materials. *Waste Biomass Valorization*. 2021;12(2):1119-1131. doi:10.1007/s12649-020-01007-3
29. Xu B, Zhao S, Shan H, Qian L, Wang J, Xin F. Effect of two boron compounds on smoke-suppression and flame-retardant properties for rigid polyurethane foams. *Polym Int*. 2022;71(10):1210-1219. doi:10.1002/PI.6403
30. Abdulateef MY, Ali MH, Hussen MA. Estimation of loads for off-grid solar photovoltaic systems Estimation of loads for off-grid solar photovoltaic systems. *Int J Power Electron Drive Syst*. 2022;13:918-925. doi:10.11591/ijpeds.v13.i2.pp918-925
31. Atsu D, Seres I, Aghaei M, Farkas I. Analysis of long-term performance and reliability of PV modules under tropical climatic conditions in sub-Saharan. *Renewable Energy*. 2020;162:285-295. doi:10.1016/j.renene.2020.08.021
32. Gholami A, Ameri M, Zandi M, et al. Impact of harsh weather conditions on solar photovoltaic cell temperature: experimental analysis and thermal-optical modeling. *Sol Energy*. 2023;252:176-194. doi:10.1016/J.SOLENER.2023.01.039
33. Mustafa RJ, Gomaa MR, Al-Dhaifallah M, Rezk H. Environmental impacts on the performance of solar photovoltaic systems. *Sustainability*. 2020;12(2):1-17. doi:10.3390/su12020608
34. Wan L, Zhao L, Xu W, Guo F, Jiang X. Dust deposition on the photovoltaic panel: a comprehensive survey on mechanisms, effects, mathematical modeling, cleaning methods, and monitoring systems. *Sol Energy*. 2024;268:112300. doi:10.1016/J.SOLENER.2023.112300
35. Kazem HA, Al-Waeli AHA, Chaichan MT, Sopian K, Gholami A, Alnaser WE. Dust and cleaning impact on the performance of photovoltaic: an outdoor experimental study. *Energy Sources Part A*. 2023;45(1):3107-3124. doi:10.1080/15567036.2023.2191064
36. Jathar LD, Ganesan S, Awasarmol U, et al. Comprehensive review of environmental factors influencing the performance of photovoltaic panels: concern over emissions at various phases throughout the lifecycle. *Environ Pollut*. 2023;326:121474. doi:10.1016/J.ENVPOL.2023.121474

37. Hussain A, Batra A, Pachauri R. An experimental study on effect of dust on power loss in solar photovoltaic module. *Renew Wind Water Sol*. 2017;4(1). doi:10.1186/s40807-017-0043-y
38. Bhallamudi R, Kumarasamy S, Karuppaiyah Sundarabalan C. Effect of dust and shadow on performance of solar photovoltaic modules: experimental analysis. *Energy Eng*. 2021;118(6):1827-1838. doi:10.32604/EE.2021.016798
39. Alves dos Santos SA, João JP, Carlos CA, Marques Lameirinhas RA. The impact of aging of solar cells on the performance of photovoltaic panels. *Energy Convers Manag X*. 2021;10(19):100082. doi:10.1016/j.ecmx.2021.100082
40. Al-Bashir A, Al-Dweri M, Al-Ghandoor A, Hammad B, Al-Kouz W. Analysis of effects of solar irradiance, cell temperature and wind speed on photovoltaic systems performance. *Int J Energy Econ Policy*. 2020;10(1):353-359. doi:10.32479/ijeep.8591
41. Pavlík M, Beňa L, Medved' D, Čonka Z, Kolcun M. Analysis and evaluation of photovoltaic cell defects and their impact on electricity generation. *Energies*. 2023;16(6):2576. doi:10.3390/en16062576
42. Hasan K, Yousuf SB, Tushar MSHK, Das BK, Das P, Islam MS. Effects of different environmental and operational factors on the PV performance: a comprehensive review. *Energy Sci Eng*. 2022;10(2):656-675. doi:10.1002/ese3.1043
43. Bernadette D, Twizerimana M, Bakundukize A, Jean Pierre B, Theoneste N. Analysis of shading effects in solar PV system. *Int J Sustain Green Energy*. 2021;10(2):47. doi:10.11648/j.ijrse.20211002.13
44. Ansari S, Ayob A, Hossain Lipu MS, Md Saad MH, Hussain A. A review of monitoring technologies for solar PV systems using data processing modules and transmission protocols: progress, challenges and prospects. *Sustainability*. 2021;13(15):8120. doi:10.3390/su13158120
45. Bhoye H, Sharma G. W Photovoltaic Solar Power Plant Design. *Int J Adv Res Electr Electron Instr Eng*. 2014;3(1):6969-6973.
46. Sahajwalla V, Hossain R. Rethinking circular economy for electronics, energy storage, and solar photovoltaics with long product life cycles. *MRS Bull*. 2023;48(4):375-385. doi:10.1557/s43577-023-00519-2
47. Mehmood KK, Khan SU, Lee S, Haider ZM, Rafique MK, Kim C. Optimal sizing and allocation of battery energy storage systems with wind and solar power DGs in a distribution network for voltage regulation considering the lifespan of batteries. *IET Renew Power Gener*. 2017;11:1305-1315. doi:10.1049/iet-rpg.2016.0938
48. Casals LC, Amante García B, Canal C. Second life batteries lifespan: rest of useful life and environmental analysis. *J Environ Manage*. 2019;232:354-363. doi:10.1016/j.jenvman.2018.11.046
49. Acharya PS, Aithal PS. Retaining the power backup of the battery and increased life span of the battery for the solar system—challenges and opportunities. *Int J Appl Eng Manage Lett*. 2020;4(2):265-274.
50. Eltamaly AM, Farh HMH. Dynamic global maximum power point tracking of the PV systems under variant partial shading using hybrid GWO-FLC. *Sol Energy*. 2019;177:306-316. doi:10.1016/J.SOLENER.2018.11.028
51. Takiso TA, Manbecho BT. Recent improvements of the PV solar energy generation performance. *Int J Recent Technol Eng*. 2021;10:117-129. doi:10.35940/ijrte.C6448.0910321
52. Chandrasekharan M. Exergy Analysis of Vapor Compression Refrigeration System Using R12 and R134a as Refrigerants. *Int J Stud Res Technol Manage*. 2014;2(4):134-139.
53. Sabry AH, Ker PINJ. DC environment for a refrigerator with variable speed compressor; power consumption profile and performance comparison. *IEEE Access*. 2020;8:147973-147982. doi:10.1109/ACCESS.2020.3015579
54. Woo S, O'neal DL. Reliability design of mechanical systems such as compressor subjected to repetitive stresses. *Metals*. 2021;11(8):1261. doi:10.3390/met11081261
55. Ahamed JU, Saidur R, Masjuki HH. A review on exergy analysis of vapor compression refrigeration system. *Renew Sustain Energy Rev*. 2011;15(3):1593-1600. doi:10.1016/j.rser.2010.11.039
56. Aized T, Rashid M, Riaz F, et al. Energy and exergy analysis of vapor compression refrigeration system with low-GWP refrigerants. *Energies*. 2022;15:7246.
57. Çengel YA, Ghajar AJ. *Heat and Mass Transfer*. McGraw-Hill Education; 2011.
58. Schubert AL, Hagemann D, Voss A, Bergmann K. Evaluating the model fit of diffusion models with the root mean square error of approximation. *J Math Psychol*. 2017;77:29-45. doi:10.1016/j.jmp.2016.08.004
59. Babarinde TO, Madyira DM. Dataset and ANFIS model prediction of the performance of graphene nano-LPG in domestic refrigerator system. *Data Brief*. 2022;44:108548. doi:10.1016/j.dib.2022.108548
60. Lei Y, Li S, Lu J, Xu Y, Yong Y, Xing D. Numerical analysis of steam ejector performance with non-equilibrium condensation for refrigeration applications. *Buildings*. 2023;13(7):1672. doi:10.3390/buildings13071672
61. Jasim MN, Alaiwi Y. Study the effect of adding heat exchanger on the refrigeration system performance. *Diyala J Eng Sci*. 2023;8716(2):1-15. doi:10.24237/djes.2023.16201
62. Aqilah F, Islam M, Juretic F, Guerrero J, Wood D, Ani FN. Study of mesh quality improvement for CFD analysis of an Airfoil. *IIUM Eng J*. 2018;19(2):203-212.
63. Toyoda N, Uematsu K, Li C, Guan Q, Vasudev H, Thakur L. Performance of hybrid nano-micro reinforced mg metal matrix composites brake calliper: simulation approach. *IOP Conf Ser Mater Sci Eng*. 2017;257:012060. doi:10.1088/1757-899X/257/1/012060
64. ANSYS. *Ansys R21.2 Fluent*. ANSYS, Inc.; 2021.
65. Yu J, Wang M, Ouyang W, An W, Liu X, Lyu H. Mesh optimization using an improved self-organizing mechanism. *Comput Fluids*. 2023;266:106062. doi:10.1016/J.COMPFLUID.2023.106062
66. Wang Y, Zheng M, Zhang J, et al. Numerical simulation study on the fluid excitation force on a nuclear fuel rod with a spacer grid. *Ann Nucl Energy*. 2023;180:109472. doi:10.1016/J.ANUCENE.2022.109472
67. Chen X, Liu J, Gong C, Li S, Pang Y, Chen B. MVE-Net: an automatic 3-D structured mesh validity evaluation framework using deep neural networks. *Comput Aided Des*. 2021;141:103104. doi:10.1016/j.cad.2021.103104
68. Serafeim A, Avgeris L, Hrissanthou V, Bellos K. Experimental and numerical simulation of the flow over a spillway. *European Water*. 2017;57:253-260.
69. Suresh K, Regalla SP. Effect of mesh parameters in finite element simulation of single point incremental sheet forming

process. *Procedia Mater Sci*. 2014;6(Icmpc):376-382. doi:10.1016/j.mspro.2014.07.048
70. Dragani H, Varevac D. Analysis of blast wave parameters depending on air mesh size. *Shock Vibr*. 2018;2018:1-18.
71. Wibolo A, Made AAI, Sudirman. Experimental study of air velocity effect of heat transfer in distillation condenser. *IOP Conf Ser Mater Sci Eng*. 2021;1175(1):012014. doi:10.1088/1757-899x/1175/1/012014
72. Alrwashdeh SS, Ammari H. Life cycle cost analysis of two different refrigeration systems powered by solar energy. *Case Stud Therm Eng*. 2019;16:100559. doi:10.1016/j.csite.2019.100559
73. Wang Y, Liu S, Nian V, Li X, Yuan J. Life cycle cost-bene fit analysis of refrigerant replacement based on experience from a supermarket project. *Energy*. 2019;187:115918. doi:10.1016/j.energy.2019.115918
74. Chen X, Chen Y, Fu L, et al. Photovoltaic-driven liquid air energy storage system for combined cooling, heating and power towards zero-energy buildings. *Energy Convers Manage*. 2024;300:117959. doi:10.1016/j.enconman.2023.117959
75. De RK, Ganguly A. Performance comparison of solar-driven single and double-effect LiBr-water vapor absorption system based cold storage. *Therm Sci Eng Progr*. 2020;17:100488. doi:10.1016/j.tsep.2020.100488
76. Pokhrel S, Kuyuk AF, Kalantari H, Ghoreishi-madiseh SA. Techno-economic trade-off between battery storage and ice thermal energy storage for application in renewable mine cooling system. *Appl Sci*. 2020 10:6022.
77. Al-Madhhachi H, Al-Najideen M. Thermal, environmental, and cost analysis of effective solar portable vaccine refrigerator by COMSOL Multiphysics. *Heat Transfer*. 2020;50(1):179-195. doi:10.1002/htj.21870
78. Kherkhar A, Chiba Y, Tlemçani A, Mamur H. Thermal engineering thermal investigation of a thermoelectric cooler based on Arduino and PID control approach. *Case Stud Therm Eng*. 2022;36:102249. doi:10.1016/j.csite.2022.102249
79. Kan A, Zhu W, Wang T, Yuan Y, Zhang X. Thermal performance assessment of cold chain chamber with vacuum insulation panel envelope layer. *Cleaner Eng Technol*. 2021;4:100157. doi:10.1016/j.clet.2021.100157
80. Gama NV, Ferreira A, Barros-Timmons A. Polyurethane foams: past, present, and future. *Materials*. 2018;11(10):1841. doi:10.3390/ma11101841
81. Batiha MA, Marachli AA, Rawadieh SE, Altarawneh IS, Almakhadmeh LA, Batiha MM. A study on optimum insulation thickness of cold storage walls in all climate zones of Jordan. *Case Stud Therm Eng*. 2019;15:100538. doi:10.1016/j.csite.2019.100538
82. Mupangwa W, Chipindu L, Ncube B, et al. Temporal changes in minimum and maximum temperatures at selected locations of Southern Africa. *Climate*. 2023;11(4):84. doi:10.3390/cli11040084
83. Tusting LS, Bradley J, Bhatt S, et al. Environmental temperature and growth faltering in African children: a cross-sectional study. *Lancet Planet Health*. 2020;4(3):e116-e123. doi:10.1016/S2542-5196(20)30037-1
84. Nemec P, Malcho M. Influence of the ambient temperature on the cooling efficiency of the high performance cooling device with thermosiphon effect. *Eur Phys J Conf*. 2018;180:02073.
85. Logeshwaran S, Chandrasekaran P. CFD analysis of natural convection heat transfer in a static domestic refrigerator. *IOP Conf Ser Mater Sci. Eng*. 2021;1130(1):012014. doi:10.1088/1757-899x/1130/1/012014
86. Raja NN, Khanderao AD. Experimental investigation on the effect of capillary tube geometry on the performance of vapor compression refrigeration system. *Asian J Eng Appl Technol*. 2016;5(2):29-35.
87. Mahmood RA, Ali OM, Noor MM. Review of mechanical vapour compression refrigeration system. Part 2: Performance challenge. *Int J Appl Mech Eng*. 2021;26(3):119-130. doi:10.2478/ijame-2021-0039
88. Quenel J, Atakan B. Heat flux in latent thermal energy storage systems: the influence of fins, thermal conductivity and driving temperature difference. *Heat Mass Transf*. 2022;58:2085-2096. doi:10.1007/s00231-022-03220-3
89. Tadesse M, Merkneh C. Design of solar PV underground water pumping system for household water consumption in Bilate Basin, Ethiopia. *Int. J. Eng. Trends Technol*. 2020;68(2):49-56. doi:10.14445/22315381/IJETT-V68I2P209
90. Umarani D, Seyezhai R, Pavithraa ST, Nandhini Priya S, Meenapriya KV. Design and implementation of solar docking station for smartphones/laptops. *Mater Today Proc*. 2021;46:10030-10035. doi:10.1016/j.matpr.2021.06.069

How to cite this article: Marwa V, Kivevele T, Kichonge B, Selemani J. Design and performance analysis of portable solar powered cooler for vaccine storage. *Energy Sci Eng*. 2024;12:4965-4990. doi:10.1002/ese3.1915

APPENDIX A

Calculations

A1. Solar panel required

$$\text{Power consumption} = 86\,\text{W} \times 6\frac{\text{hr}}{\text{day}} = 516\frac{\text{Wh}}{\text{day}}. \tag{A1}$$

$$\text{Total photovoltaic cell needed} = 516\frac{\text{Wh}}{\text{day}} \times 1.3 = 670\frac{\text{Wh}}{\text{day}}. \tag{A2}$$

where 1.3 is taken as energy lost in the system.

$$\text{Total photovoltaic cell panel capacity} = \frac{670.8}{3.43}\ \frac{\text{Wh}}{\text{day}} = 197.3\ W_{\text{p}}, \tag{A3}$$

where 3.43 is taken as the panel generation factor.[89,90]

$$\text{Number photovoltaic cell panel needed} = \frac{197.3\ W_p}{200\ W_p} \approx 1\ \text{module}. \quad \text{(A4)}$$

A2. Solar battery needed

$$\text{Total battery size} = \frac{86\text{W} \times 18\text{h} \times 1\text{days}}{0.8 \times 12\text{V}} = 161.25\text{Ah}. \quad \text{(A5)}$$

Battery size available in the market = 85Ah.

$$\text{Number of battery required} = \frac{\text{total battery size}}{\text{battery size}} = \frac{161\text{Ah}}{85\text{Ah}} = 1.89 \approx 2\ \text{batteries}. \quad \text{(A6)}$$

A3. Size of charge controller

$$\text{Current} = \frac{\text{power}}{\text{voltage}} = \frac{200\text{W}}{12\text{V}} = 16.6\text{A} \times 1.25 = 20.75\text{A}. \quad \text{(A7)}$$

A4. Compressor power

$$\text{Compressor power} = \dot{m} \times W_c = 0.0055\frac{\text{kg}}{\text{s}} \times 36840\frac{\text{J}}{\text{kg}} = 184.2\text{W}. \quad \text{(A8)}$$

1 horsepower = 746Watts.

$$\text{Compressor to be used} = \frac{184.2\text{W}}{746\text{W}} = 0.2\ \text{horsepower} = \frac{1}{5}\text{hp}. \quad \text{(A9)}$$

A5. Condenser power

$$\text{Condenser load } (Q_L) = 0.0055\frac{\text{kg}}{\text{s}}\dot{} \times 187825\frac{\text{J}}{\text{kg}} = 1037.83\text{W}. \quad \text{(A10)}$$

A6. Evaporator power

$$\text{Evaporator power } (Q_E) = 0.0055\frac{kg}{s}\dot{} \times 150985\frac{J}{kg} = 830.42\text{W}. \quad \text{(A11)}$$

A7. Coefficient of performance (COP)

$$\text{COP} = \frac{h_1 - h_4}{h_2 - h_1}, \quad \text{(A12)}$$

$$\text{COP} = \frac{830.42\text{W}}{184.2\text{W}} = 4.5. \quad \text{(A13)}$$